

Perturbed orbital motion of regolith around Asteroids

MSc Thesis Report

Abhishek Agrawal



PERTURBED ORBITAL MOTION OF REGOLITH AROUND ASTEROIDS

MSc Thesis Report

by

ABHISHEK AGRAWAL

to obtain the degree of Master of Science
at the Delft University of Technology.

Student number: 4416600
Thesis committee: Dr. Ir. D.J. Scheeres, University of Colorado, Boulder, supervisor
Ir. R. Noomen, TU Delft, supervisor
Dr. Ir. , TU Delft
Ir. , TU Delft

An electronic version of this thesis is available at <http://repository.tudelft.nl/>.



Cover image credit: Adopted from European Southern Observatory. Artist's Impression of the binary asteroid Antiope.

"If you wish to make an apple pie from scratch, you must first invent the universe."

Carl Sagan

PREFACE

After 45 years since the day man landed on the Moon, mankind created history, yet again. For the first time ever, a spacecraft was put into an orbit around a comet and a lander was deployed to its surface. This was the Rosetta mission; launched in March 2004, the spacecraft took an astonishing 10 years to travel to the comet 67P/Churyumov-Gerasimenko, finally arriving at the comet in August 2014. This is an immense achievement for the scientists and engineers involved in the Rosetta mission because space missions to small irregular bodies in our solar system, both comets and asteroids, pose significant dynamical challenges. For scientists, missions to comets and asteroids are of great interest since in-situ exploration of these small bodies can provide insight into the birth of our Solar System and answer some very important and fundamental questions such as those about the origins of life on Earth. Now even the private space industry is interested in these small bodies, such as in mining the vast reserves of untapped natural resources within the small bodies. For a student, designing and assessing orbits around a small irregular body, and in our case an asteroid, turns out to be one of the toughest problems in astrodynamics, making it a perfect research topic for an MSc Thesis.

This report serves to be a *Literature Study* in the framework of the Master's program at the Faculty of Aerospace Engineering, Delft University of Technology. It paves way for the upcoming thesis project, where the actual research work shall be carried out. I am grateful I could do this literature study under the supervision of my supervisor Ir. Ron Noomen and with support from Dr. Jinglang Feng. Their experience in the subject matter has been of tremendous help to me. In writing this report, I have tried my very best to ensure that the material in the report is presented in a manner which is pleasant to read and understand. I hope you can gain some valuable knowledge from reading this report.

*Abhishek Agrawal
Delft, August 2016*

CONTENTS

Preface	v
List of Symbols	ix
List of Acronyms	xi
1 Introduction	1
I Motivation	5
2 Heritage	7
2.1 Past Missions	7
2.1.1 NEAR-Shoemaker	7
2.1.2 Hayabusa	8
2.2 Future Missions	9
2.2.1 Hayabusa-2	10
2.2.2 OSIRIS-REx	10
2.3 State of the art / Literature Review	10
3 Thesis Objectives	11
II Numerical Simulation Results	13
4 Results	15
4.1 Regolith launched from the longest edge of the asteroid	15
4.1.1 Dynamics without Solar perturbations	15
4.1.2 Dynamics with Solar perturbations	15
Bibliography	51
Appendices	53
A Extra Figures	55

LIST OF SYMBOLS

LATIN LETTERS

Symbol	Units	Description
r	m	position vector magnitude
\mathbf{r}	m	position vector
U	m^2/s^2	Gravitational potential

GREEK

Symbol	Units	Description
α	m	Largest semi-major axis of tri-axial ellipsoid shaped asteroid

LIST OF ACRONYMS

- AU** Astronomical Unit
- CCW** Counter-Clockwise
- CKBO** Classical Kuiper-Belt Objects
- EHAO** Extremely-High Altitude Orbit
- ESA** European Space Agency
- HAO** High Altitude Orbit
- JAXA** Japan Aerospace Exploration Agency
- LAF** Low-Altitude Flyover
- LAO** Low Altitude Orbit
- MAB** Main Asteroid Belt
- MAO** Medium Altitude Orbit
- MBO** Main-Belt Objects
- NASA** National Aeronautics and Space Administration
- NEA** Near-Earth Asteroids
- NEAR** Near Earth Asteroid Rendezvous
- NEO** Near-Earth Objects
- OSIRIS-REx** Origins, Spectral Interpretation, Resource Identification, Security, Regolith Explorer
- SCI** Small Carry-on Impactor
- SDO** Scattered Disk Objects
- SKG** Strategic Knowledge Gap
- SRP** Solar Radiation Pressure
- STBE** Solar Third Body Effect
- TAG** Touch-And-Go
- TNO** Trans-Neptunian Objects
- UHAO** Ultra-High Altitude Orbit

1

INTRODUCTION

At the dawn of the nineteenth century, Italian astronomer Giuseppe Piazzi was engrossed in observing the Taurus constellation to update a star catalog. On January 1 1801, atop the Palermo observatory in Sicily, he observed a light which wasn't mentioned in the catalog. He followed the strange light for a few more nights, eventually realizing that he had discovered a small planet between Mars and Jupiter. He named the minor planet *Ceres* and it became the first of its kind to be discovered by humans. Broadly speaking, it became the first *asteroid* to ever be discovered (Cunningham 2016). Soon after this discovery, three other minor planets were discovered in the gap between Mars and Jupiter. *Pallas* was discovered in 1802, followed by *Juno* in 1804, and finally *Vesta* in 1807. After the discovery of *Ceres* and *Pallas*, renowned astronomer William Herschel realized that these are a new species of celestial bodies and proposed to call them *asteroids* (which in Greek meant *star-like*) instead of *minor planets*. For nearly 40 years after the discovery of *Vesta*, no additional discoveries were made. Then once again in the second half of the nineteenth century, astronomers started discovering more and more of these asteroids until they realized that there is a whole *belt* of it between Mars and Jupiter (Bottke 2002).

Asteroids are rocky, airless celestial bodies in our Solar System that orbit the Sun and are quite small in size compared to the planets. They can be viewed as remnants of the processes that formed the inner planets of our Solar System (NASA, "Asteroids: In depth"). Asteroids are mostly irregularly shaped with a few exceptions, like Ceres, that have a nearly spherical shape. Figure 1.1 provides a view on the different morphologies of asteroids (NASA, "Asteroids: In depth"). They are typically categorized based on their location in the Solar System. A large number of asteroids are found in the region between Mars and Jupiter and are called as MBO (Main-Belt Objects). A relatively smaller number of asteroids, called NEA (Near-Earth Asteroids), have orbits that are very close to and/or crosses the heliocentric orbit of Earth. Asteroids at the L_4 and L_5 Lagrange points of Jupiter, sharing its orbit around the Sun, are termed as *Trojans*. Then we have *Centaurs*, asteroids whose orbit lies between or crosses that of the Giant planets in our Solar System. The fifth and the final category is of the TNO (Trans-Neptunian Objects) i.e. asteroids with orbit beyond that of Neptune and reaching as far as the Oort cloud (De Pater et al. 2015). The distribution of asteroids in the inner and outer Solar system is shown in Figure 1.2.

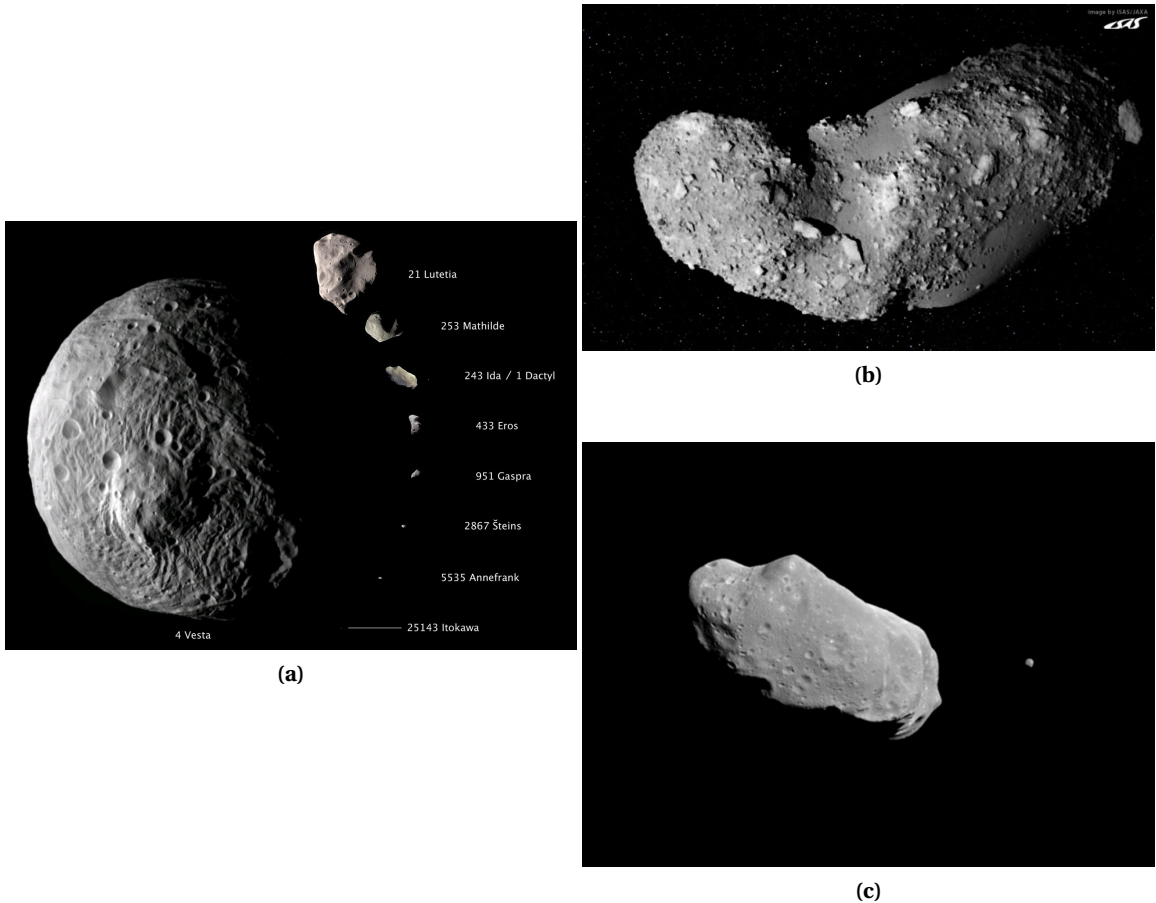


Figure 1.1: Satellite imagery depicting different morphologies of asteroids. (a) depicts the size and shape variations amongst a few known asteroids, (b) asteroid Itokawa with its rocky and rough surface, (c) asteroid Ida with its moon Dactyl orbiting around it ([NASA, "Asteroids: In depth"](#)).

Due to their extremely small sizes, asteroids can not have high internal pressures and temperatures which means that they could have potentially preserved the early chemistry of our Solar System (Kubota et al. 2006). This makes them a valuable source for us to understand about the history and origin of our Solar System. It is hypothesized that during the early years of Earth's formation, carbon-based molecules and other volatile materials which serve as the basic building-blocks of life, could have been delivered to Earth through asteroid impacts ([JPL, "SSD"](#)). Finally, some asteroid types are rich in resources and contain vast supplies of precious metals (Kargel 1994) and water (Morbidelli et al. 2000), which could potentially be mined and used to aid further exploration and colonization of our Solar System ([JPL, "SSD"](#)). Thus in light of this, asteroid exploration, both in-situ and ex-situ, have gained significant importance not only amongst the scientific community but amongst the private space industry as well, with more and more future missions being planned for these small bodies. The NEAR (Near Earth Asteroid Rendezvous) spacecraft launched by NASA (National Aeronautics and Space Administration) in 1996, as part of their *Discovery* program, became the first spacecraft in history to orbit an asteroid (433 Eros) and eventually land on it. The spacecraft spent almost a year around Eros, providing extended and comprehensive observations of surface morphology, shape, internal structure and physical properties of the asteroid (Plockter et al. 2002). The Hayabusa mission (formerly MUSES-C) by JAXA (Japan Aerospace Exploration Agency) entered into orbit around asteroid Itokawa in 2005 and became the first mission to sample the surface of an asteroid, which were subsequently returned to Earth for analysis in 2010 (Yano et al. 2006). These missions have substantially increased our knowledge about the small bodies in our Solar System.

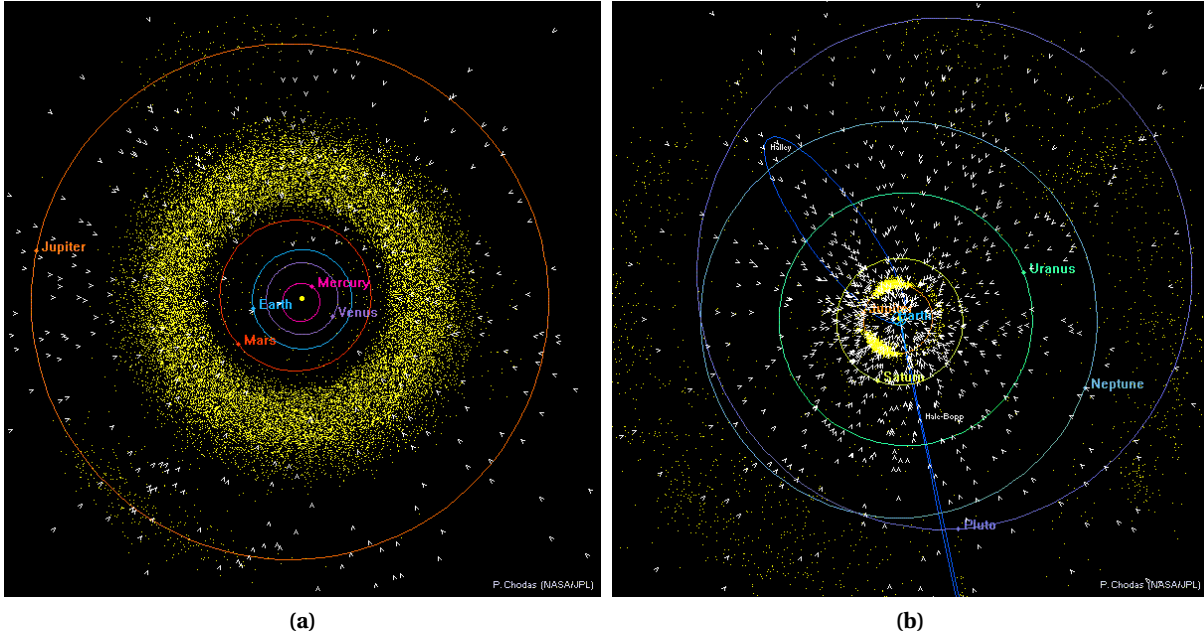


Figure 1.2: Distribution of asteroids in (a) inner Solar System and (b) outer Solar System. Asteroid locations are shown by yellow-colored dots whereas the white-colored wedges pointing towards the Sun represent the comets. The diagrams are based on the small-bodies catalogued up until November 2016 ([JPL, "SSD"](#)).

Two more asteroid rendezvous missions launched quite recently, are however, of particular interest to this thesis. Following the success of Hayabusa, JAXA launched another sample return mission called Hayabusa-2 to asteroid 1999 JU3, scheduled to be in orbit around it by mid-2018. It will perform a 1.5 year long close-proximity operation at the asteroid that includes surface sample acquisition, which will eventually be returned to Earth in a capsule, and a 2 [m] wide cratering event to observe the sub-surface (Tsuda et al. 2013). The OSIRIS-REx (Origins, Spectral Interpretation, Resource Identification, Security, Regolith Explorer) mission by NASA, directed towards asteroid Bennu and scheduled to enter into an orbit around it in late-2018, will also retrieve a surface sample and return it back to Earth. It will employ a TAG (Touch-And-Go) maneuver to acquire a sample within a 1.5 month long scheduled sampling period (Berry et al. 2013). Both the missions are aiming to find out if organic material, volatiles and water itself were brought to Earth by such asteroids. These mission employ techniques for sample acquisition that could potentially disturb the state of regolith on the surface of the asteroid and loft it into an orbit. For the success of these and all other missions in the future, it is imperative to understand the complex dynamical environment around asteroids, not only for space crafts, but also for the orbital motion of lofted regolith. NASA has identified the acquisition of such information as a SKG (Strategic Knowledge Gap) for NEO (Near-Earth Objects), specifically article III-A-1: *Expected particulate environment due to impact ejecta* in [NASA, "SKG"](#).

The study of lofted regolith around an asteroid is by no means a new research topic. In the studies done previously (Richter et al. 1995; Lee 1996; Scheeres et al. 1996; Scheeres et al. 2000; Korycansky et al. 2004; Yáñez et al. 2014), we have witnessed certain minor drawbacks such as not always accounting for gravity and Solar perturbations together, or using an approximated analytical method to understand the dynamical environment that falls short on obtaining the entire spectra of initial

conditions that could lead to different final outcomes (re-impact, escape or temporary capture) for lofted regolith, or not considering different size and density for the lofted regolith, and finally not considering the local direction with respect to a rotating asteroid in which the regolith is ejected. This thesis, thus, aims to include all of these shortfalls in a single study, and by using numerical simulation techniques, to add more fidelity in understanding what happens to regolith when it is lofted from the surface of an asteroid.

The study of orbiting regolith is important for understanding the displacement of material on surface of the asteroid in case of natural or spacecraft induced impact cratering events. In case of the latter, the ejecta from the impact cratering event could pose serious threat to spacecraft and/or its instruments. By knowing the orbital behavior of regolith in advance, mission designers can make informed decisions on the trajectory design of spacecraft to avoid or reduce failure scenarios. Another important benefit that comes from a study like this is in the field of asteroid mining, whereby the regolith's orbital motion and final fate can be exploited to sort different materials in real time. The results from this thesis will thus aid mission designers in planning future asteroid missions and in answering the following research question:

Can we explain the orbital behavior and eventual fate of lofted regolith around an asteroid in presence of perturbations?

The structure of this report is as follows:

Part I

Motivation

2

HERITAGE

In the past, there have been multiple spacecraft missions to the small bodies in our Solar System which have collectively increased our understanding about them. While a large majority of these have been asteroid fly-by scenarios, a few have also been rendezvous missions (ESA 2014). This chapter will provide an overview on few of these missions followed by a brief literature review which shall be of interest to the thesis at hand. This will help us in justifying the research objectives mentioned in Chapter 3. Section 2.1 will discuss the asteroid rendezvous missions which have already taken place, Section 2.2 will discuss future rendezvous missions, and finally, Section 2.3 will discuss the state-of-the-art.

2.1 PAST MISSIONS

In all the history of space exploration there have been only three spacecraft missions that have rendezvoused with asteroids. In chronological order these are: NASA's NEAR-Shoemaker mission to asteroid Eros, JAXA's Hayabusa mission to asteroid Itokawa, and NASA's Dawn mission to asteroids Vesta and Ceres (Scheeres 2016). Out of these, only NEAR and Hayabusa had direct contact with the small bodies and acquired high-resolution imagery of surface regolith.

2.1.1 NEAR-SHOEMAKER

The NEAR-Shoemaker (henceforth NEAR) mission was launched in 1996 and rendezvoused with Eros in 2000. Its operational phase around the asteroid continued for about a year during which it obtained several high-resolution images of the surface and collected comprehensive measurements to estimate its internal mass distribution, shape model, gravity and spin state amongst other observations (Scheeres 2016). The bulk density of Eros was estimated to be $2.67 \pm 0.03 [g/cm^3]$ and its mass to be $(6.6904 \pm 0.003) \times 10^{15} [kg]$. The rotation state was estimated to be $1639.38922 \pm 0.00015 [\text{deg/day}]$ which gives a rotational period of about 5.27 [hrs] (Miller et al. 2002). On 25 October 2000, NEAR executed a LAF (Low-Altitude Flyover) over Eros in which it acquired several high-resolution images that helped in understanding the surface morphology. The images confirmed the existence of a substantial amount of regolith on the surface with a typical thickness value of tens of metres over the bedrock, except of course on steep slopes. The regolith was found to be highly complex, in that it varied from fine material to metre-sized ejecta blocks (Veverka et al. 2001a). Robinson et al. 2001 estimates the size of the finer regolith to be around 1.0 [cm] or smaller from images that had a resolution of 1.2 [cm] per pixel. Figure 2.1 depicts the regolith morphology in one of the high-resolution imaging sequences from the LAF (Veverka et al. 2001b).

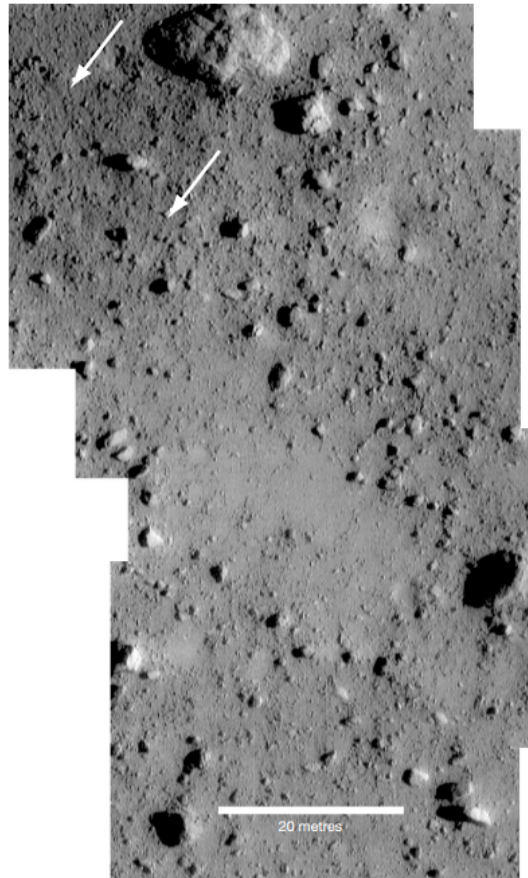


Figure 2.1: Mosaic of high-resolution images depicting the nature of regolith on the surface of Eros (Veverka et al. 2001b).

2.1.2 HAYABUSA

The Hayabusa spacecraft was launched by JAXA in 2003 and it arrived at asteroid Itokawa in 2005. After arrival, it performed close-proximity operations around the asteroid for approximately 3 months during which several measurements were taken to estimate the shape, mass, topography and elemental composition of the asteroid. During this period, the spacecraft also collected samples from the surface of the asteroid that were eventually returned back to Earth in 2010. The measurements at Itokawa estimated its mass to be 3.51×10^{10} [kg] and its bulk density to be 1.9 ± 0.13 [g/cm^3] (Fujiwara et al. 2006).

Two distinct types of terrains can be recognized on Itokawa, one which is rough and rich in boulders and the other which is smooth and mostly flat. This distinction can easily be seen in Figure 2.2. The smooth regolith regions, that account for approximately 20% of Itokawa's surface, composed of fragmented debris with grain sizes ranging from sub-centimetre to centimetre scales. One of the smooth regolith regions, called Muses Sea and from where the sample was also acquired, even consisted of a few metre-sized boulders that were hypothesized to have landed in the region as secondary ejecta (Miyamoto et al. 2006). The rougher terrain on Itokawa, which has a very sharp boundary with the smoother regolith filled regions (as evident in Figure 2.2), consists of boulders that range upto tens of metres in size (Fujiwara et al. 2006).

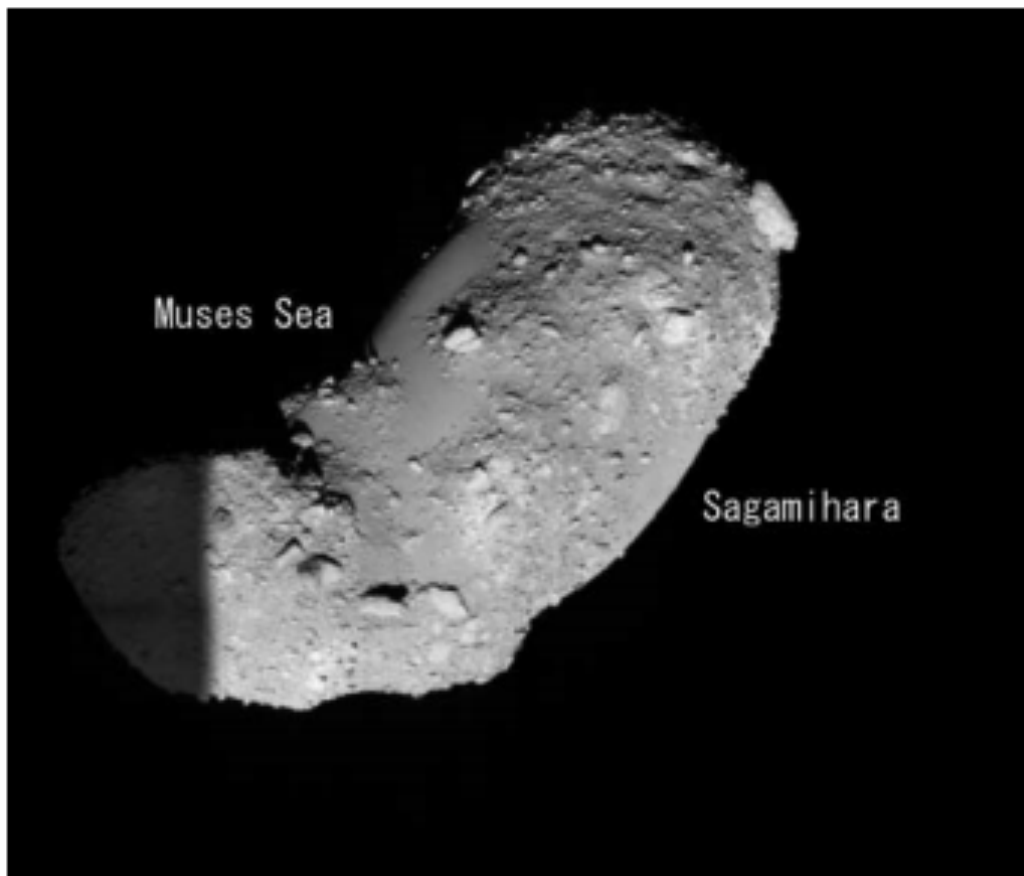


Figure 2.2: Image of Itokawa taken from a 7 [km] altitude depicting the nature of regolith on its surface. Muses Sea and Sagamihara are the two distinct smooth regolith regions on the asteroid (Fujiwara et al. 2006).

Hayabusa employed an *impact sampling mechanism* that would work across various types of terrains, from hard bedrock to fine regolith. The spacecraft consisted of a long cylindrical sampling horn with a conical tip. When the tip of the horn touched the surface of the asteroid, the deformation in the horn's fabric was detected by a laser range finder and within 0.3 [s] of this event, a 5.0 [g] projectile was fired towards the surface with a velocity of 300 [m/s] and the resultant ejecta was collected by the sampler (Yano et al. 2004). Yano et al. 2006 presents data from the sampling experiments that were performed on ground in 1g and micro-gravity environments. The experiments revealed that, for the projectile hitting at normal impact angles in micro-gravity, the impact ejecta mass of particles greater than 1.0 [cm] ranged from 2 - 11 [g] whereas for particles less than 1.0 [mm] the ejecta mass ranged from 100 - 10000 [g]. The impact target consisted of various analog materials from glass beads to lunar regolith simulant and an experiment like is a nice indicator of how artificial impact events can displace significant amount of fragmented debris on an asteroid.

2.2 FUTURE MISSIONS

We will now discuss two missions, Hayabusa-2 by JAXA and OSIRIS-REx by NASA. Both are currently en route to their respective target asteroids and after orbit insertion, they shall perform operations to collect surface samples.

2.2.1 HAYABUSA-2

Hayabusa-2 is the second asteroid sample return mission by JAXA, which to a significant extent, shares the successful technical legacy of Hayabusa. The target asteroid of the former is *1999 JU3* which is suspected to contain organic matter and hydrated minerals. A successful sample return from this asteroid may thus help us in understanding the origin of life and/or water on Earth. The spacecraft will enter into an orbit around its target by mid-2018, after which it will perform close-proximity operations for 1.5 years. The mission will entail 3 touchdowns for sample acquisition and a cratering event to observe the subsurface of the asteroid. The sampling mechanism is based on that of Hayabusa and each sampling attempt has the potential to acquire samples in the order of 100 [mg]. The samples are sealed-off and transported back to Earth in a re-entry capsule. The cratering operation is performed by a SCI (Small Carry-on Impactor). The SCI is deployed by the spacecraft at an altitude of 500 [m] and after a preset time, a detonation accelerates it to about 2 [km/s] prior to impact. It is estimated that this will result in a crater of about 2 [m] wide. Prior to the detonation of SCI, the spacecraft will move to a safe location on the opposite side of the asteroid from the impact point to avoid damage from impact ejecta and/or debris from the detonation. Apart from these, the spacecraft will perform other in-situ operations to characterize the asteroid and will also deploy a lander and three miniature rovers for technology demonstration (Tsuda et al. 2013).

2.2.2 OSIRIS-REX

OSIRIS-REx is part of NASA's New Frontiers program and will travel to NEA *1999 RQ₃₆*, also known as Bennu. The mission, amongst other scientific objectives, will return a regolith sample back to Earth that may provide insight into the initial states of planetary formation as well as answer questions on the origins of life. Since Bennu is a NEA, the sample collection and subsequent analysis will provide us information on asteroids that could potentially impact Earth. The spacecraft was launched in 2016 and is expected to reach its target by the end of 2018 (Berry et al. 2013). The asteroid has a semi-major axis of 1.126 [AU] which makes it an easily accessible asteroid as far as distance is concerned. But more than that, Bennu falls under the category of asteroids that are rich in volatiles and could potentially be related to objects that brought the seeds of life to Earth. Initial observations of Bennu through ground based telescopes, the Spitzer Telescope, the Arecibo Observatory and other assets revealed an abundance of regolith on the surface with grain sizes ranging from 4 - 8 [mm]. OSIRIS-REx will acquire the regolith sample using a TAG mechanism which uses pressurized Nitrogen gas to force the loosely held regolith into a collection chamber. The sampling will occur in 2020 and it will be retrieved on Earth in 2023 (Lauretta et al. 2012).

2.3 STATE OF THE ART / LITERATURE REVIEW

3

THESIS OBJECTIVES

Part II

Numerical Simulation Results

4

RESULTS

4.1 REGOLITH LAUNCHED FROM THE LONGEST EDGE OF THE ASTEROID

The results that we'll discuss in this section pertain to the case of regolith launched from the longest edge of the asteroid, modeled as an ellipsoid.

4.1.1 DYNAMICS WITHOUT SOLAR PERTURBATIONS

...to be added later...

4.1.2 DYNAMICS WITH SOLAR PERTURBATIONS

In this case, the simulation accounted for perturbations from the irregular gravity field of the asteroid, the SRP (Solar Radiation Pressure), and the STBE (Solar Third Body Effect). Within this category, there are 4 distinct sets of simulations, each for a particle with different Area-to-Mass ratio. These are mentioned in Table 4.1. The material with a density of $3.2 \text{ [g/cm}^3]$ is low-density Olivine (Magnesium Iron Silicates) and the one with $7.5 \text{ [g/cm}^3]$ is Iron-Nickel alloy (Garcia-Yarnoz et al. 2014). We have chosen these two types of materials based on the surface composition analysis of asteroid Eros, an S-Type asteroid, from the NEAR-Shoemaker data. S-Type asteroids, from reflectance spectral analysis, are commonly known to have minerals like Olivine, Pyroxene, and Fe-Ni (Iron-Nickel) metal (Nittler et al. 2001). Thermo-spectral analysis of regolith on Eros reveals that it is rich in Olivine and is found to be more abundant than Pyroxene (McCoy et al. 2001). The mineral Olivine has also been discovered on Itokawa, another S-Type asteroid, through transmission electron microscope analysis of samples returned by the Hayabusa spacecraft (Keller et al. 2014). Eros also contains Fe-Ni but it is significantly separated from the Silicates (Olivine and Pyroxene) within the regolith (Nittler et al. 2001). Evans et al. 2001 analyzed elemental composition of NEAR-Shoemaker's landing site on Eros, based on which, it presents several arguments for relatively lower abundance of Fe (Iron) on the surface of Eros. One of the arguments hypothesizes that different grain sizes and density of Fe-Ni from Olivine could have resulted in the metal to get separated from the Silicates, either spatially or for it to sink down in the lower depths of the regolith. In light of this, we are considering regolith comprising of only Olivine and Fe-Ni, to distinguish between their orbital behavior and final fate upon being lofted from the surface of Eros. Veverka et al. 2001a analyzed high resolution surface images of Eros captured by NEAR-Shoemaker on a low-altitude flyover. It argued the build-up of a heterogeneous and complex regolith that comprised of material ranging from fine particles all the way up to metre-sized ejecta blocks. Veverka et al. 2001a argues that while there is an abundance of large ejecta blocks across the surface, the much finer regolith occupies mostly the low-lying topographies, i.e., inside large craters on the surface of Eros. The latter was termed as ponded deposits. Robinson et al. 2001 argues, from high resolution images (1.2 [cm] per

pixel) of ponded deposits at Eros, that the grain size of regolith would be around 1.0 [cm] or below. Thus based on this extreme spectra of regolith composition at Eros, we shall also consider regoliths with varying densities and grain radii (each grain is assumed to be spherical). These are listed in Table 4.1. The particles are listed in decreasing order of area-to-mass ratio. We considered coarse regolith of 10 [cm] radius as well, the motivation for which comes from the size of the ejecta blocks generated from the impact of NEAR-Shoemaker on Eros's surface. Robinson et al. 2001 notes that there are several 10 [cm] ejecta blocks around the NEAR-Shoemaker impact site. Thus, ejecta size of 10 [cm] in radii is justified for this study in the context of an asteroid exploration or exploitation mission.

Table 4.1: Particle Area-to-Mass ratios

Code	Particle radius [cm]	Density [g/cm ³]	Area-to-Mass ratio [m ² /kg]
LoGSP-1	1.0	3.2	0.0234
LoGSP-2	1.0	7.5	0.01
LoGSP-3	5.0	3.2	0.0047
LoGSP-4	5.0	7.5	0.002
LoGSP-5	10.0	3.2	0.0023
LoGSP-6	10.0	7.5	0.001

The initial conditions for lofting each type of regolith are varied in the same manner and are mentioned as follows. The asteroid revolves around the Sun in an equatorial circular orbit at a distance of 1.0 AU (Astronomical Unit). Four different initial Solar phase angles were considered for the simulation – 45.0, 135.0, 225.0 315.0 [deg], to account for the four different quadrants where the Sun could be with respect to the asteroid. For each case in Table 4.1, a total of 72 particles were launched from the surface of the asteroid, each in a different direction (defined using the launch declination and azimuth angles). The launch declination angle, measured from the zenith, was kept constant at 45.0 [deg] for all the particles. The launch azimuth, measured CCW (Counter-Clockwise) from the direction pointing to north, was varied at a resolution of 5.0 [deg] starting from 0.0 [deg] all the way up to 355.0 [deg]. Each particle was launched, in their specified direction, with different velocities ranging from 1.0 [m/s] to 16.0 [m/s] (measured with respect to the asteroid-centric rotating frame) at a resolution of 1.0 [m/s]. So basically, every combination of an initial Solar phase angle, initial launch azimuth, and initial launch velocity corresponds to a unique trajectory for a single particle of a given Area-to-Mass ratio; Thus amounting to a total of 4608 unique trajectories for each regolith type.

The simulations were subjected to run for a maximum of 270.0 [days] and were terminated earlier if a particular trajectory resulted in escape or surface re-impact. This number was obtained by looking at the close-proximity operational time periods of exploration missions to small bodies of our solar system. We wanted a maximum simulation time in the context of a man-made mission and hence this approach was taken. We accounted for four missions, two from the past and two planned for the future, which have direct contact with a small body as part of their mission and continued the mission around the small body afterwards (hence, not just disposal and/or fly-by). These are the Philae (Rosetta), Hayabusa, Hayabusa-2, and the OSIRIS-REx mission. The close-proximity design operation time period for Philae lander was 3 months (Biele et al. 2008), 3 months for Hayabusa (Kawaguchi et al. 2003), 18 months for the Hayabusa-2 mission (Tsuda et al. 2013), and finally 12 months for the OSIRIS-REx mission (Lauretta et al. 2012). The average of all of this comes out to be 9.0 months, which is what we have considered to be the maximum simulation time. In this regard, we are also categorizing orbital behavior that does not result in escape or re-impact in those 270 days, as capture orbits.

We now present a detailed analysis for one of the regolith types, particle LoGSP-1, because

Olivine is the most abundant of the regolith types found on Eros and among the different grain sizes for Olivine, LoGSP-1 offers the maximum area-to-mass ratio. A larger value for area-to-mass ratio means a relatively larger effect of SRP on the regolith which makes it more interesting since for a detailed analysis we want to see how SRP (as well as STBE in general) affects the orbital motion of regolith.

CASE LoGSP-1

Figure 4.1 gives a distribution of particles (henceforth the term particle and regolith shall be used interchangeably without any implication in change of its meaning) for each of the three different final fates for the regolith i.e. capture, re-impact, and escape, for different initial launch velocities and initial Solar phase angles. Irrespective of the initial Solar phase, initial launch velocities from 1.0 to 3.0 [m/s] results in particles launched in all directions to eventually re-impact the asteroid's surface. Similarly, for initial launch velocities ranging from 14.0 to 16.0 [m/s], we see that the particles always manage to escape the gravitational attraction of the asteroid. However, there is one exception to the former statement, a single particle launched with a velocity of 14.0 [m/s] at a launch azimuth of 90.0 [deg] and at an initial Solar phase angle of 315.0 [deg], re-impacts the asteroid's surface. It is interesting to note that the launch azimuth of the particle is such that it is launched in a direction that is directly opposite to the direction of rotation of the asteroid. Launch velocities from 4.0 to 13.0 [m/s] show a mixed behavior and the final fate distribution trend does not vary drastically for different initial Solar phase angles.

The number of capture cases is far less than those for escape and re-impact. For initial Solar phase of 225.0 [deg], there are no cases of regolith being captured in orbit around the asteroid. All capture cases, arranged in order of increasing launch azimuth angle, are listed in Table 4.2. It is interesting to note that all capture cases result from when the particle is launched in a direction which is against the direction of rotation of the asteroid, bar one exception which is case index-11 in Table 4.2. The capture cases which represent symmetry in terms of the launch azimuth angle are

Table 4.2: Initial conditions that resulted in temporary orbital capture of regolith around the asteroid. Particle code LoGSP-1.

Index	Launch azimuth [deg]	Launch velocity [m/s]	Initial Solar phase angle [deg]
1	5.0	5.0	315.0
2	10.0	9.0	135.0
3	15.0	8.0	45.0
4	45.0	12.0	45.0
5	45.0	10.0	315.0
6	135.0	12.0	45.0
7	135.0	10.0	315.0
8	165.0	8.0	45.0
9	170.0	9.0	135.0
10	175.0	5.0	315.0
11	185.0	5.0	135.0

highlighted with the same color in Table 4.2. This symmetric behavior results from the combination of two factors. First, the Sun's motion relative to the asteroid is not in an inclined plane, and secondly, the particles are launched from the equatorial tip of the ellipsoid shaped asteroid, which is a point of symmetry on the ellipsoid. The capture cases will be discussed in detail a bit further ahead.

Regolith final fate histogram, Ellipsoid longest edge

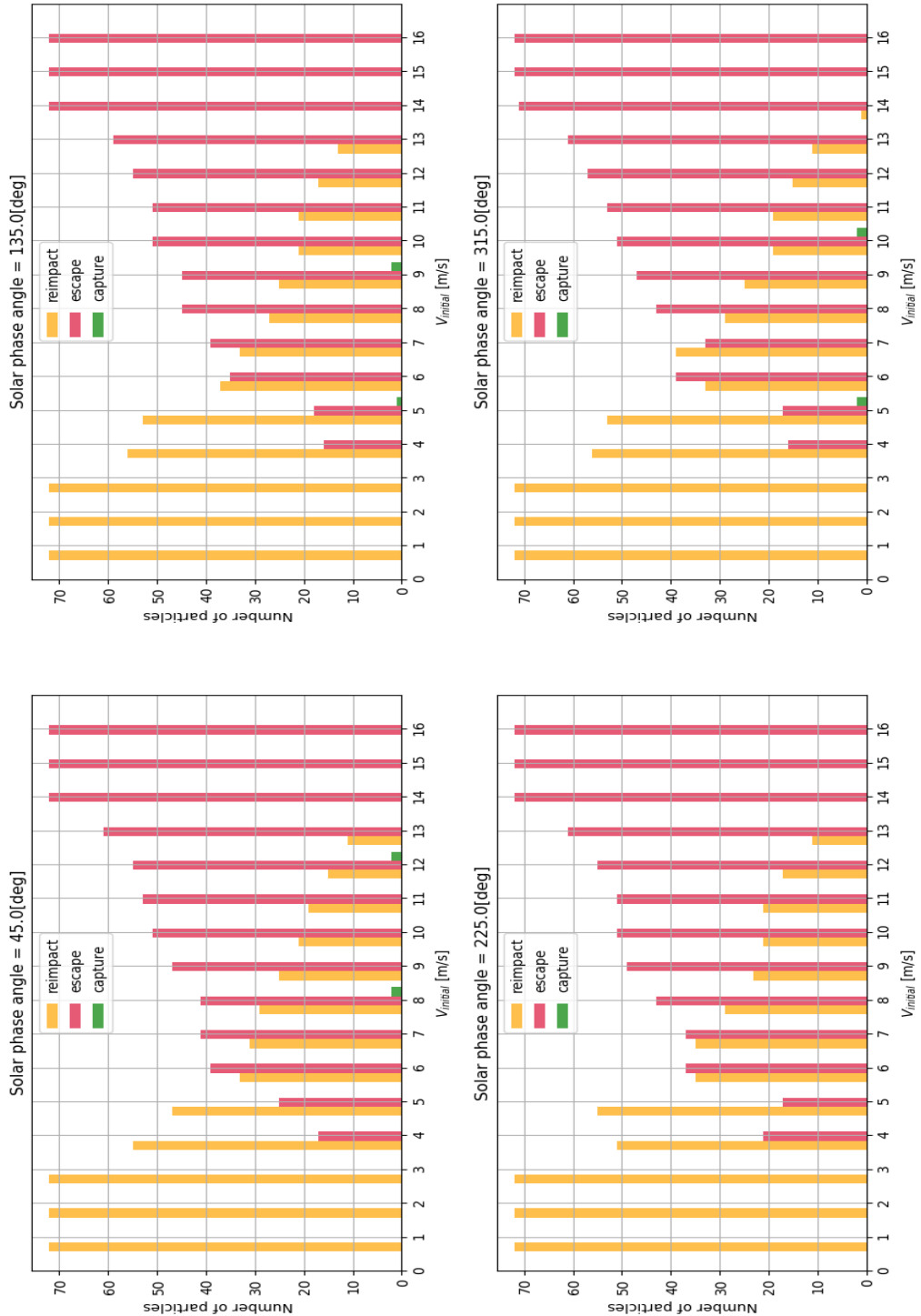


Figure 4.1: Histogram showing the number of particles that re-impact, escape, or get captured around the asteroid, for different initial launch velocities. Particle code LoGSP-1.

Figure 4.2 depicts the surface distribution of regolith that re-impacts the surface when launched from the same location with different velocities and different initial Solar phase angles. The launch location is in the centre of the map, Latitude 0.0 [deg] and Longitude 0.0 [deg]. The particle distribution is the same for regions close to the launch point and for lower launch velocities up until 8.0 [m/s]. A similarity in distribution pattern is also observed around Longitude -150.0 [deg] for launch velocity of 9.0 [m/s] and around Longitude 150.0 [deg] for launch velocity of 10.0 [m/s] for the four Solar phase angles. The distribution pattern, for all launch velocities and initial Solar phases, is also symmetric about the equator. Again, the reason for this is the same as mentioned earlier for the symmetry in capture cases in Table 4.2. Keeping the launch direction and velocity constant, we see that the distribution of regolith that re-impacts the surface does not change drastically with varying initial Solar phase angles, except for a relatively few cases. This is much easily observed in a plot of Range from the launch direction to the re-impact point versus launch azimuth for different velocities as shown in Figure 4.3.

We haven't shown the range to re-impact point plots in Figure 4.3 for all launch velocities because the intention here is to show the qualitative behavior, which can be achieved by considering only a subset of the launch velocities that result in a re-impact scenario. The very first thing we observe is that as the launch velocity increases, the range of launch azimuth over which the regolith re-impacts the surface reduces because a higher velocity allows the regolith to enter a higher orbit (as it attains a relatively higher energy) and reduces the probability of a re-impact. Even as the velocity increases, we see that the azimuths that result in a re-impact are the ones in which the regolith is launched in a direction that is opposite to the asteroid's rotation direction. This makes sense since the regolith's energy would be reduced the most in this scenario compared to all other launch directions, thereby increasing the chances of a re-impact.

Now the primary purpose of the plots in Figure 4.3 (combined with Figure 4.2) is to depict the qualitative effect of Solar perturbations, for varying initial Solar phase angles, on the re-impact behavior of regolith compared to the case when no Solar perturbations are considered. For launch velocities of 4.0, 7.0 and 10.0 [m/s], we see that the Solar perturbations do not affect the re-impact location for cases when the particle is launched in directions opposite to that of the asteroid's rotation. However, we do see few exceptions to the former statement, most noticeably in the case of 7.0 [m/s]. But for the majority of cases where the re-impact location remains unchanged, we see from Figure 4.4, that these particles spend less than 3.0 [Hrs] in orbit which is not enough time for the Solar perturbations to act and have any significant impact on the dynamics of the particles. So in essence this is what's happening here - Particles when launched in a direction that is opposite to that of the asteroid's rotation, even at relatively high velocities such as 10.0 [m/s], loose enough energy to stay in a relatively lower orbit (see Figure A.1) where the gravitational force of the asteroid is significantly stronger than any of the Solar perturbations and as the particle spends a very short time in orbit before re-impact, the Solar perturbations do not get enough time to affect the particle's orbit and hence the particle re-impacts the same location as it would have when no Solar perturbations were considered in the simulation. For the lower launch velocities of 4.0 and 7.0 [m/s], the differences in re-impact locations are more pronounced when the regolith is launched in the same direction as that of the asteroid's rotation. Particles gain relatively higher energy in this case, enter a higher orbit and spend enough time in there for the Solar perturbations to affect its motion. For the case of the launch velocity of 13.0 [m/s] in Figure 4.3, the velocity is high enough such that the particle does not loose enough energy when launched opposite to the asteroid's rotational direction and is able to enter a relatively higher orbit (see Figure A.1) and stay there for a relatively longer time, as seen in Figure 4.4, which results in the Solar perturbations affecting the orbital motion and eventually the re-impact location of the regolith.

Regolith crash map for multiple launch velocities
Ellipsoid longest edge

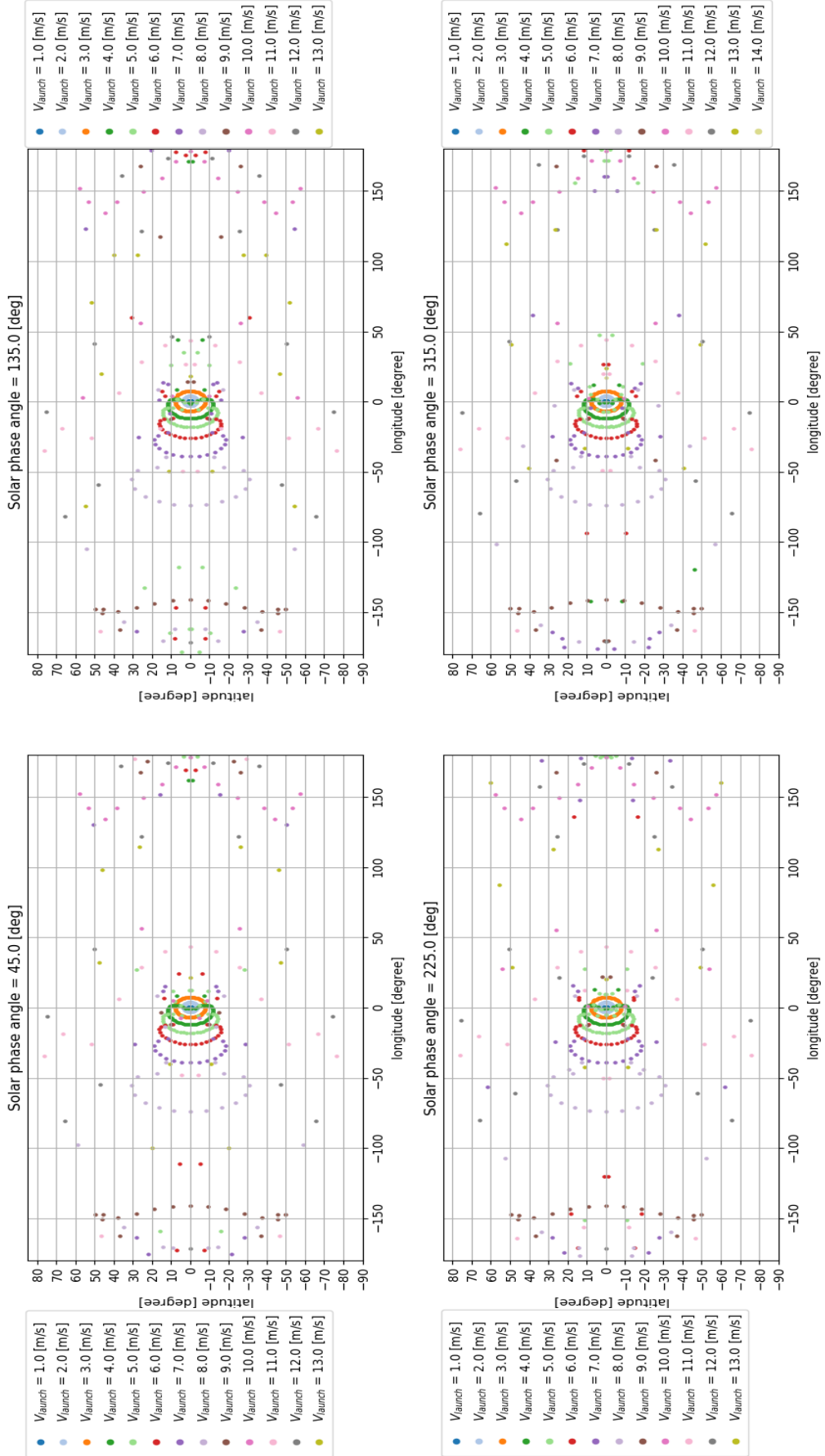


Figure 4.2: Surface distribution of re-impacted regolith for different launch velocities. The launch location is latitude: 0.0 [deg], longitude: 0.0 [deg]. Particle code LoGSP-1.

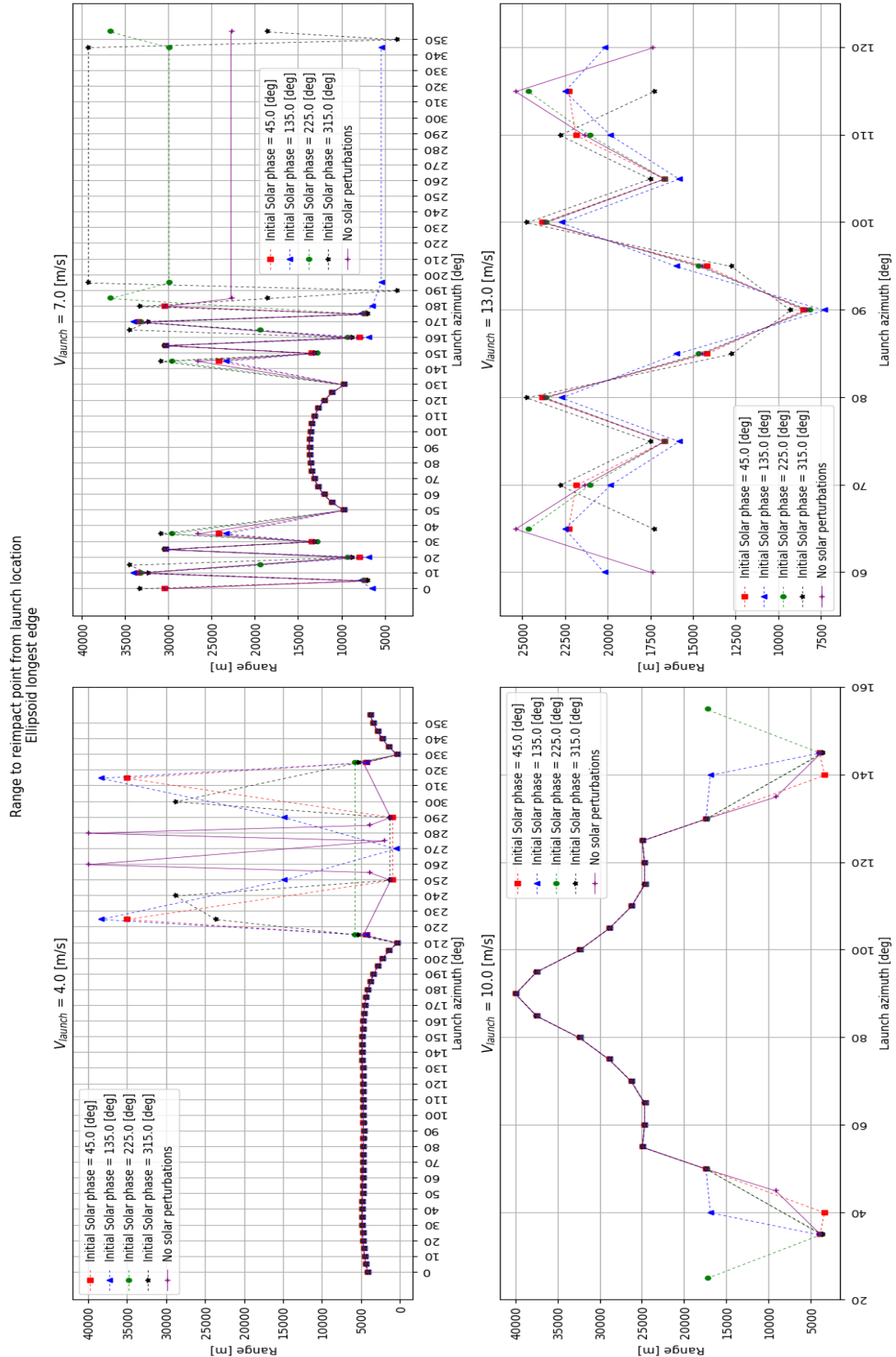


Figure 4.3: Range to re-impact location from the launch point for different velocities. Particle code LoGSP-1.

Time for regolith to reimpact, Ellipsoid Longest edge

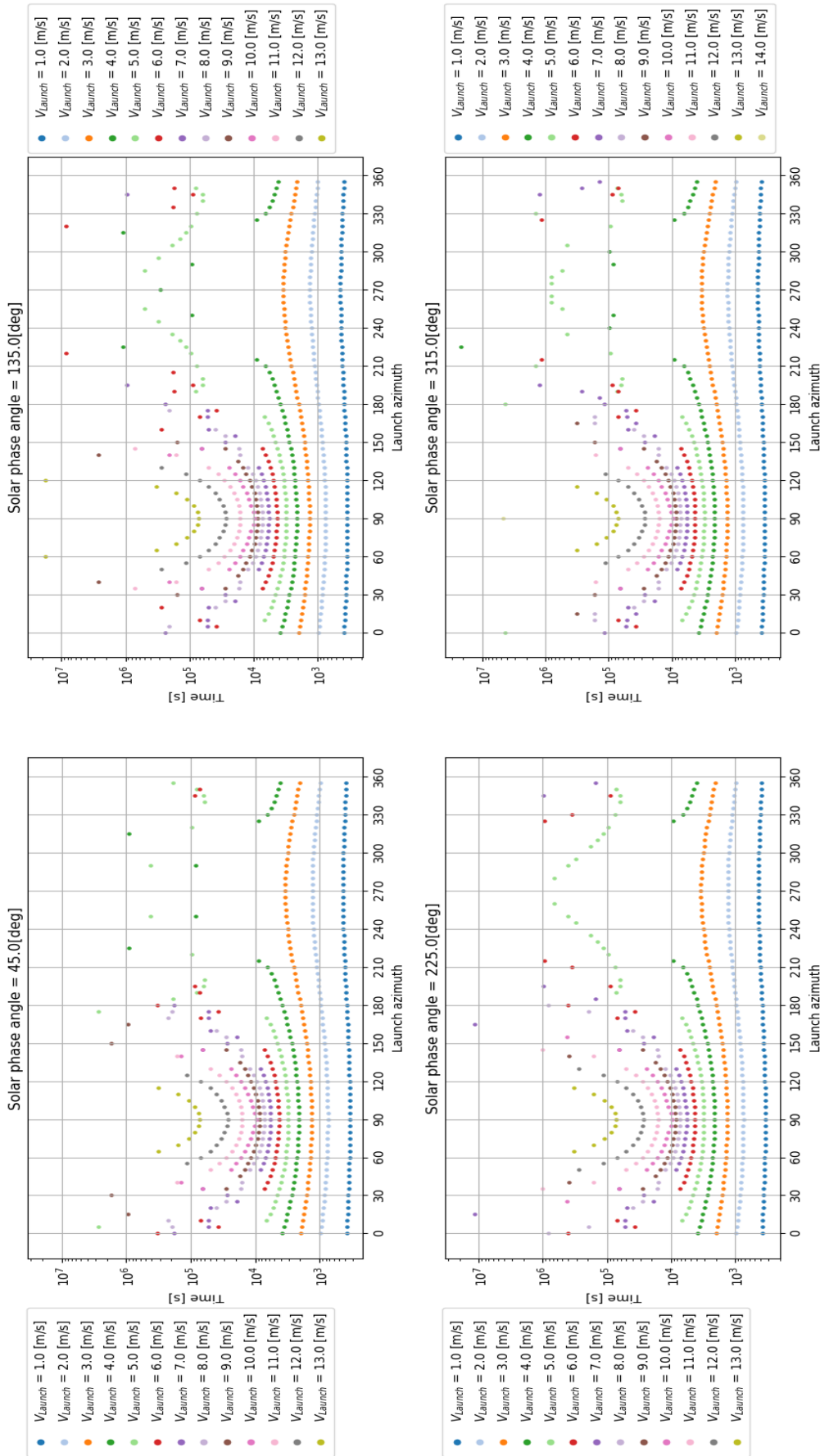


Figure 4.4: Time taken by regolith at different velocities and launch directions to re-impact with the surface of the asteroid. Particle code LoGSP-1.

We shall now look at the cases where the lofted regolith gets (temporarily) captured in orbit by the asteroid. The initial conditions for all capture cases, for the current particle size and density, were mentioned earlier in Table 4.2. Figure 4.6 depicts the progression in orbital range of the temporarily captured regolith. The straight lines in the plot are used to mark the different altitude regimes. These are the LAO (Low Altitude Orbit), MAO (Medium Altitude Orbit), HAO (High Altitude Orbit), UHAO (Ultra-High Altitude Orbit), and EHAO (Extremely-High Altitude Orbit). These altitude regime definitions are not from well defined standards, but instead were arbitrarily chosen as integer multiples of the longest semi-major axis, α , of the tri-axial ellipsoid shaped asteroid. The definition for these altitude regimes is given in Table 4.3.

Table 4.3: Altitude regimes and their definitions

Altitude regime	Definition
LAO	Asteroid surface to $2 \times \alpha$
MAO	$2 \times \alpha$ to $3 \times \alpha$
HAO	$3 \times \alpha$ to $5 \times \alpha$
UHAO	$5 \times \alpha$ to $7 \times \alpha$
EHAO	Above $7 \times \alpha$

The purpose of plotting data as shown in Figure 4.6 was to look for any patterns or periodicity, if they existed, and to see if particles in temporary capture scenario remain closer to the asteroid or further away from it. The symmetry as explained for initial conditions mentioned in Table 4.2 can also be seen in Figure 4.6, for example, regolith launched with velocity of 8.0 [m/s] and launch azimuth of 15.0 [deg] (shown by the purple curve in the top plot in Figure 4.6) shows the same behavior as that of regolith launched with the same velocity and 165.0 [deg] launch azimuth (shown by the green curve in the bottom plot in Figure 4.6). Another thing we see from the plot is that, apart from case number 11 in Table 4.2, the captured regolith stay in the higher altitude regions for most part and only briefly do they fall within the MAO and LAO region. We shall now look at atleast three cases from Figure 4.6 in a bit more detail to understand the effect of Solar perturbations by comparing these cases with their counterparts from the simulation where Solar perturbations were omitted.

Of all the cases shown in Figure 4.6 or Table 4.2, the one with a launch velocity of 10.0 [m/s] and launch azimuth of 45.0 [deg] results in a re-impact scenario when Solar perturbations are omitted but the same initial conditions lead to a temporary capture orbit when perturbations were added for an initial Solar phase angle of 315.0 [deg]. Every other initial condition for the capture cases had otherwise resulted in an escape situation when simulations were conducted without the Solar perturbations. The 3D trajectory plot in two different views for the former case are shown in Figure 4.7 (see Figure A.2 also for the 3D trajectory representation in body fixed frame). The 2D trajectory for the same is shown in Figure 4.8 in inertial frame and in Figure A.3 in the asteroid centric rotating frame or the body frame. The web-link or URL for the trajectory animation of the particle (in inertial frame and in XY plane only) can be found in Figure 4.5.



Figure 4.5: 2D trajectory animation (XY Plane) of capture regolith for case number 5 in Table 4.2. Particle code LoGSP-1. Scan the QR code to view the animation or use the following web-link: <https://youtu.be/oZDhDo5CIsk>

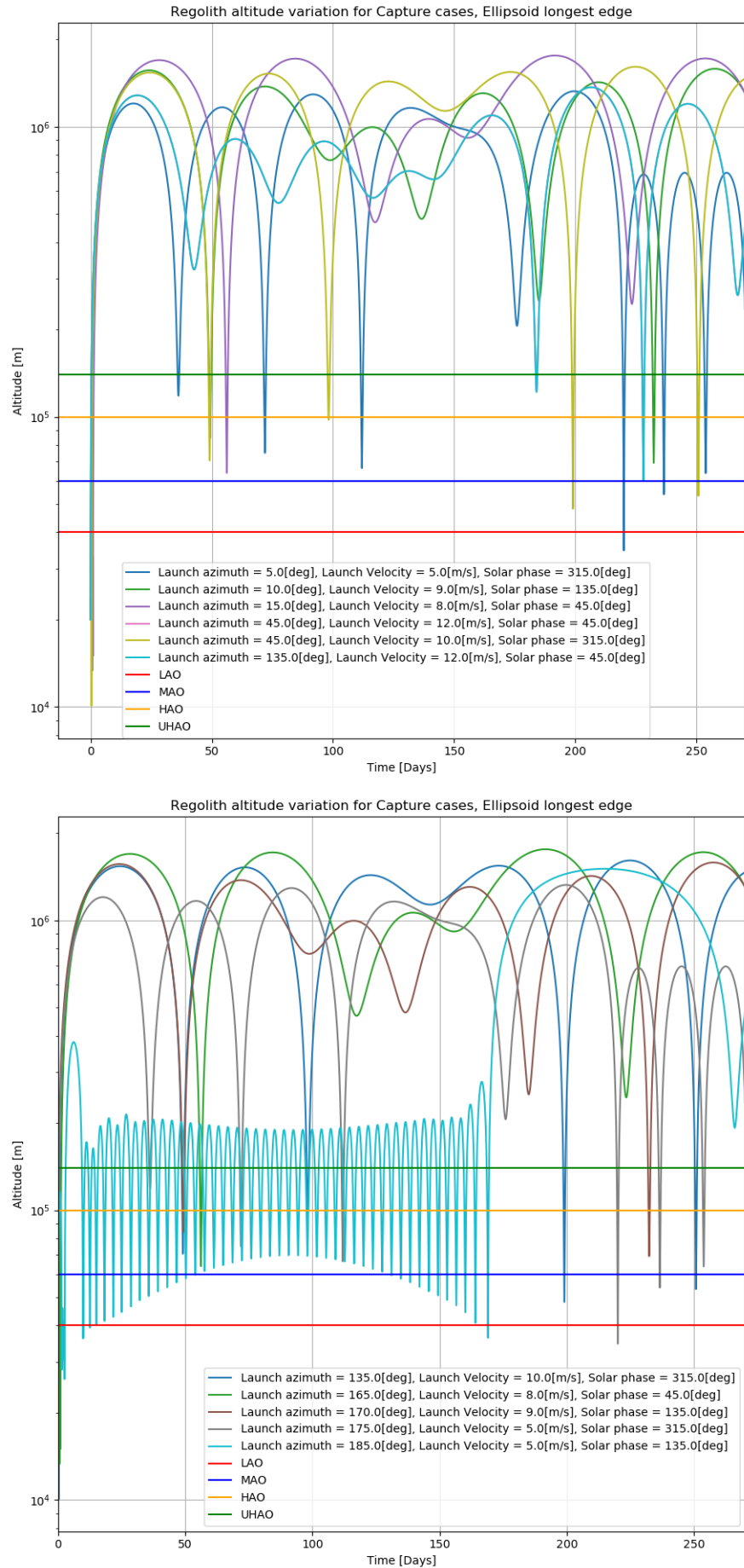
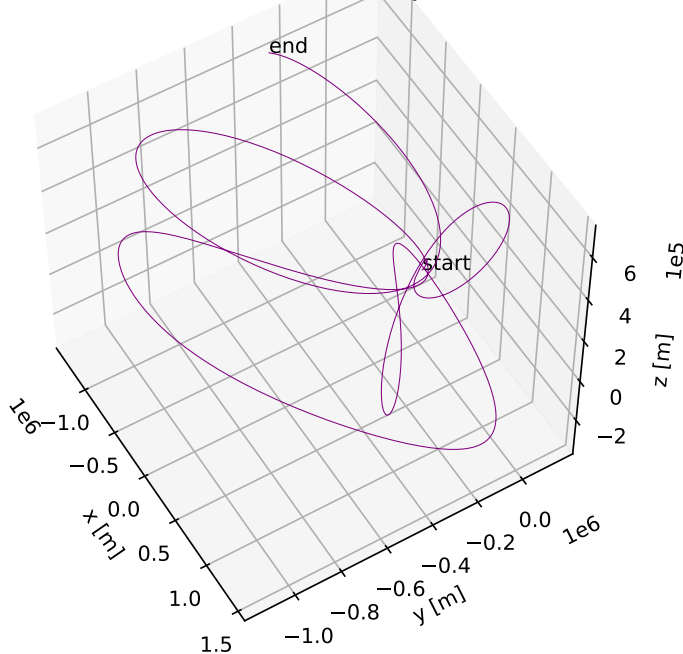


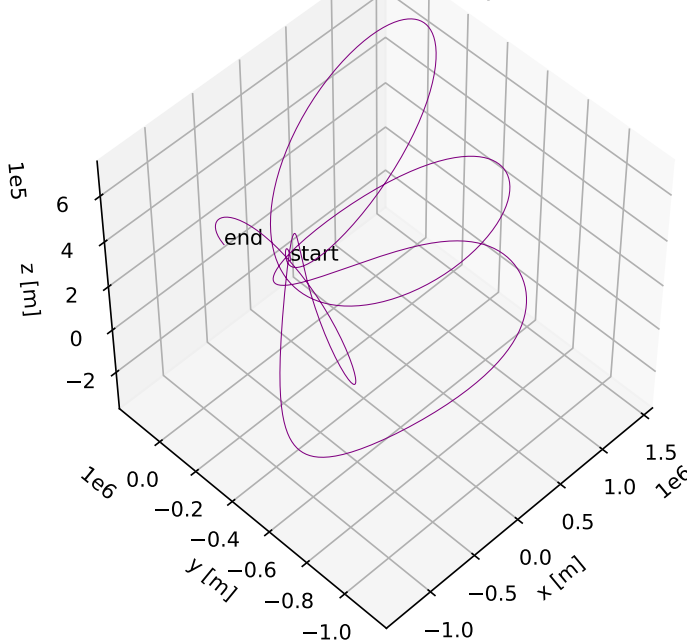
Figure 4.6: Orbital range progression with time for temporary capture scenarios. Particle code LoGSP-1.

Ellipsoid longest edge, Inertial frame trajectory
 $V_{\text{launch}} = 10.0 \text{ [m/s]}$, Launch azimuth = 45.0 [deg], Solar phase = 315.0 [deg]
Time = 0.0 to 270.0 [days]



(a)

Ellipsoid longest edge, Inertial frame trajectory
 $V_{\text{launch}} = 10.0 \text{ [m/s]}$, Launch azimuth = 45.0 [deg], Solar phase = 315.0 [deg]
Time = 0.0 to 270.0 [days]



(b)

Figure 4.7: 3D inertial frame trajectory of capture regolith for case number 5 in Table 4.2 in two different viewing angles.
Particle code LoGSP-1.

Note that in the trajectory animation in Figure 4.5 (and any other animation included henceforth) the particle is made to skip several data points in between along the trajectory when it is far away from the asteroid, just to reduce the length of the animation. So because of this, the particle appears to be moving faster when it is away from the asteroid but this is not true. For the exact velocity of the particle, the reader should look at the velocity magnitude indicator within the animation itself.

The animation shows that the particle reverses its direction of motion twice in its entire course. To visualize how this is happening in 3D, look at Figure 4.7. The reason for this can be understood by looking at the direction of the perturbing acceleration, the gravitational acceleration vectors, and the combined effect of all accelerations acting on the particle. The direction of SRP and STBE are shown in Figure 4.9 and that of the net effect of the two is shown in Figure 4.10a. In the trajectory simulator, the gravity model (triaxial ellipsoid model) computes the acceleration in the rotating frame. We calculated the direction of the gravitational acceleration in inertial frame in post-simulation analysis assuming a point-mass model by considering the fact that when the regolith is far-away from the asteroid, its gravity field would appear as that of a point-mass gravity source. The gravitational acceleration vectors are shown in Figure 4.10b. The net acceleration acting on the particle is then shown in Figure 4.11. All acceleration vectors are shown along those parts of the trajectory where the magnitude of SRP acceleration is of the same order of magnitude as that of the gravitational acceleration. However, the magnitude of the STBE acceleration is always 1.0 order of magnitude smaller than the gravitational acceleration for those very same points along the trajectory, but is still significant. We do not show the vectors for the entire trajectory for two reasons; first, when close to the asteroid the direction of these vectors would reduce the clarity of the plot and, second, we want to discuss the effect of the perturbations when the particle is far away from the asteroid because then they are as significant as the gravitational force.

In Figure 4.8, the trajectory loops numbered 1 and 2 (XY plane), is where the particle's direction of motion gets reversed. If we look at Figure 4.9a, we see that the direction of the SRP vector is consistent with how the particle changes its direction of motion. This, however, does not mean that the SRP is the sole actor responsible for how the particle's motion eventually turns out to be (and we will see this in detail shortly). The direction of STBE, as shown in Figure 4.9b, however, does not directly tell us on how the particle's motion would change as it progresses through its trajectory. STBE is always an order of magnitude smaller than SRP for the points shown in the two plots and its direction is not consistent with how the particle changes its direction of motion but its contribution to the capture scenario is significant (we will see the effect of removing STBE shortly). The direction of the net perturbing acceleration, shown in Figure 4.10a, shows us exactly how and where the motion of the particle is directed. Especially when we look at trajectory loops 1 and 2 in Figure 4.8, we can see that the net perturbing vector is acting in the direction that is consistent with how the particle changes its orbital motion. Now looking at these plots that we just discussed, a question that arises is that - why did the particle remain in a temporary capture orbit, and for example not escape especially when the net perturbing acceleration was acting opposite to the direction of asteroid such as in trajectory loop number 3 in Figure 4.8? The answer to this is found by looking at the direction of gravitational attraction in Figure 4.10b and the total acceleration (i.e. the net effect of gravity and perturbations) acting on the particle in Figure 4.11. Although the gravitational acceleration has the same order of magnitude as that of the Solar perturbations when the particle is far away from the asteroid, we see that the net effect of the two is towards the asteroid and hence prevents the particle from escaping.

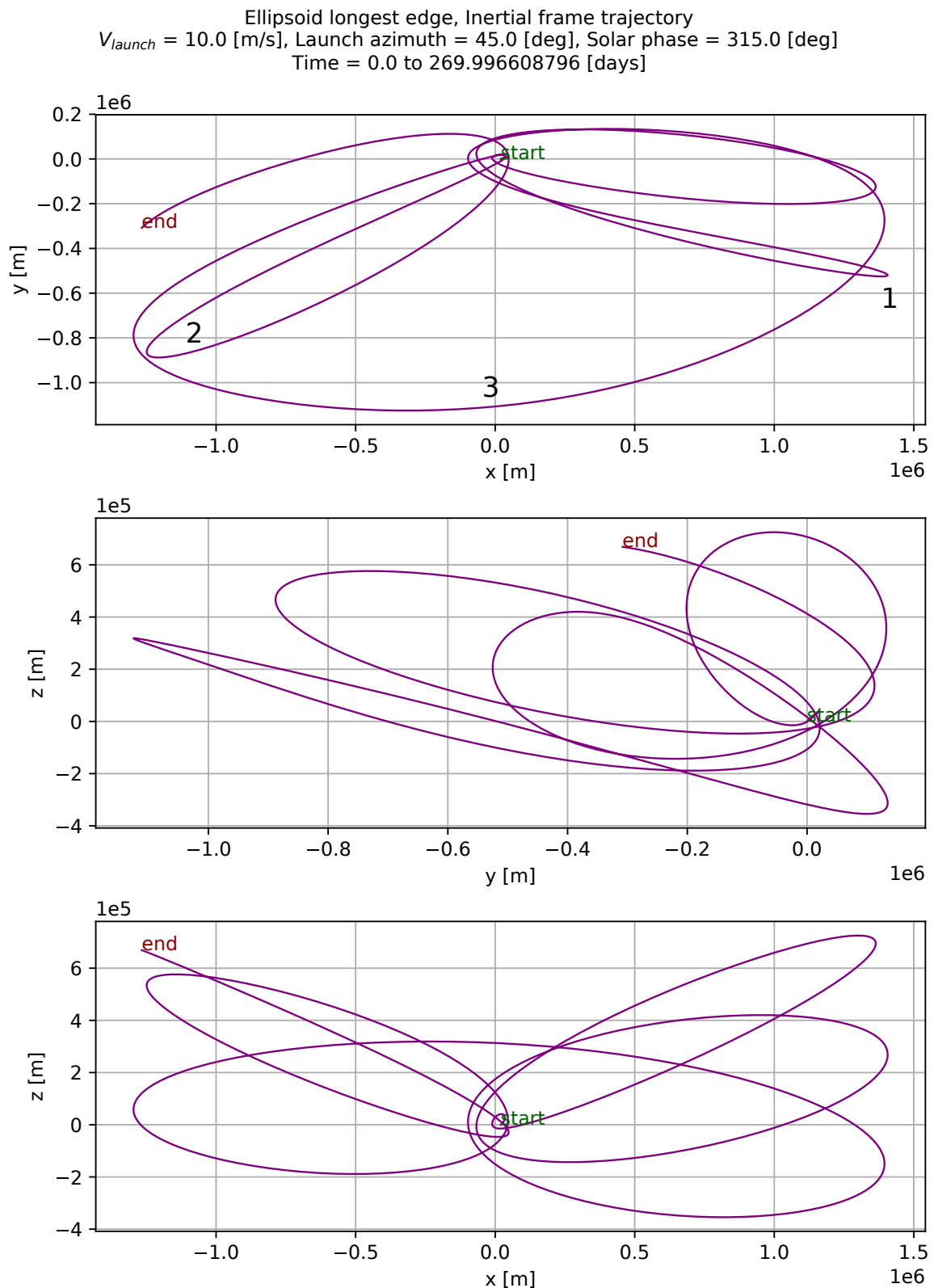


Figure 4.8: 2D inertial frame trajectory of capture regolith for case number 5 in Table 4.2. Particle code LoGSP-1.

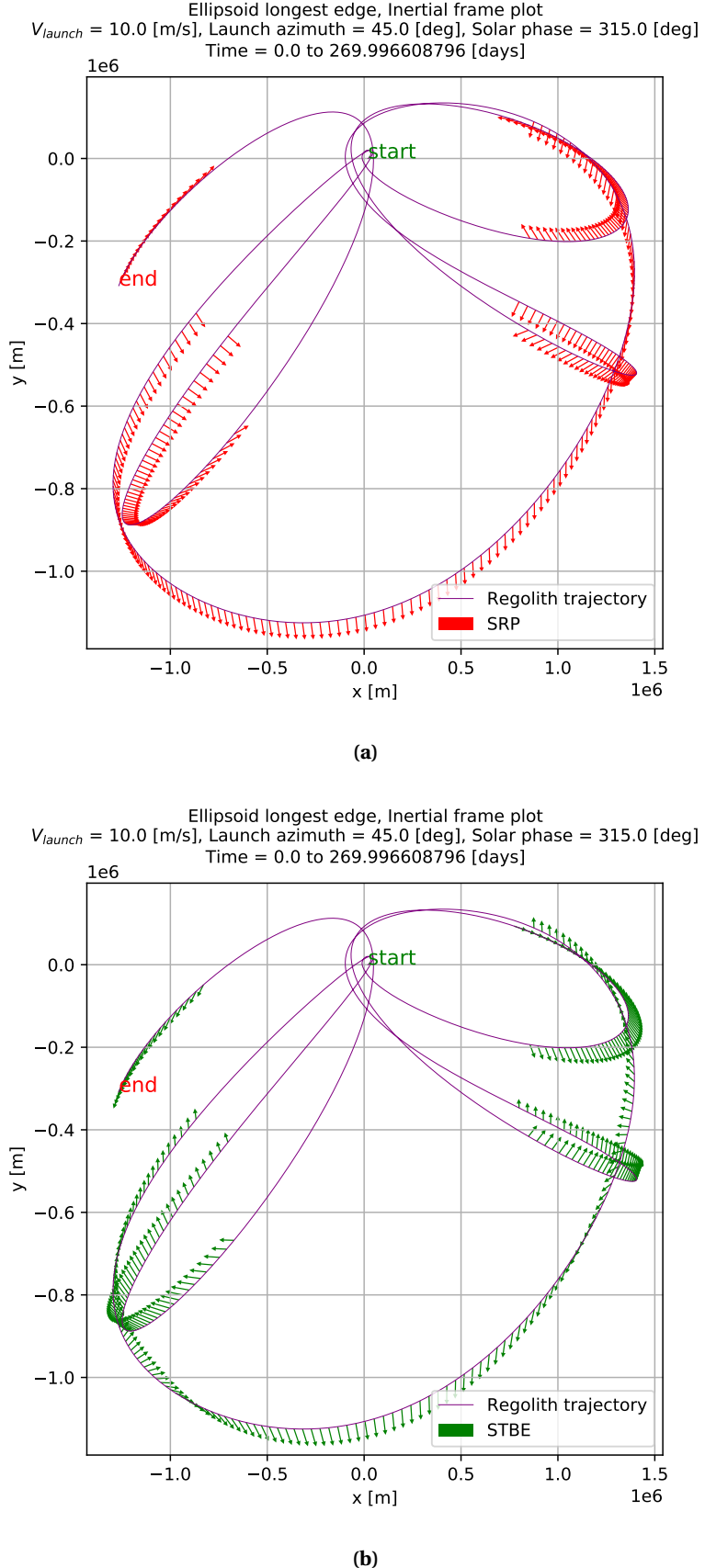
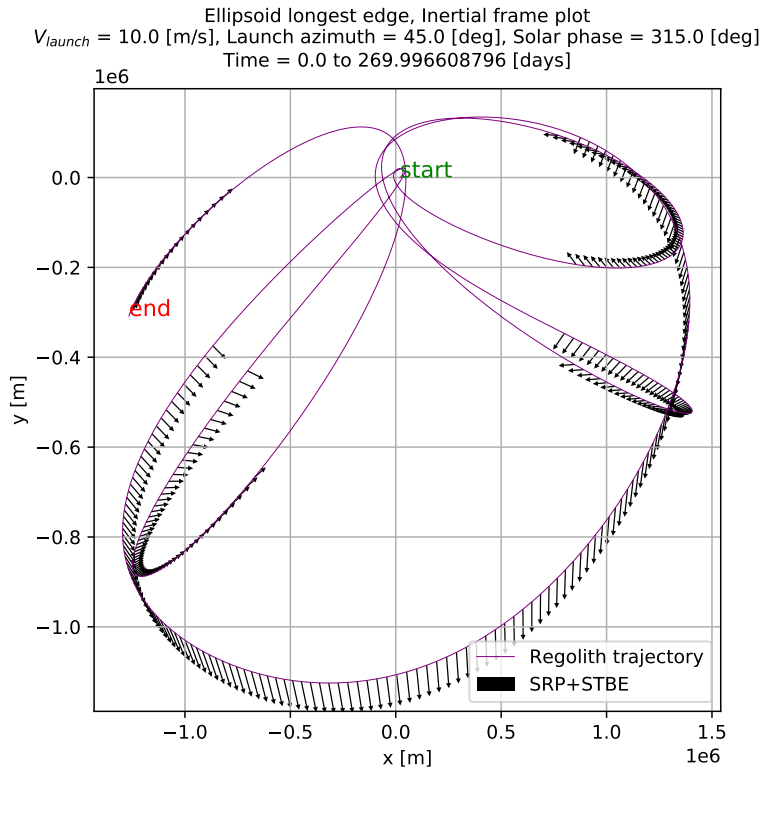
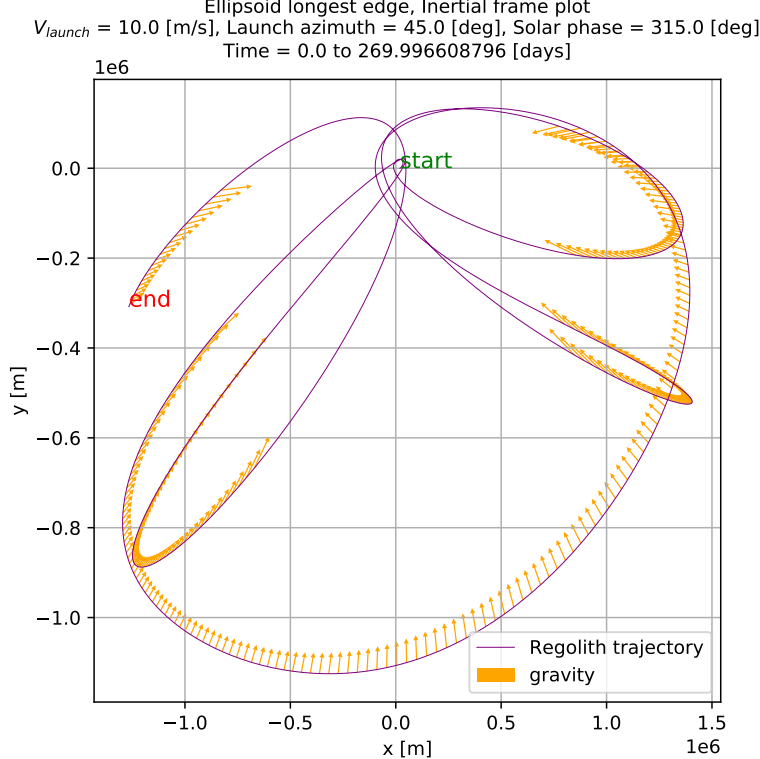


Figure 4.9: 2D trajectory of capture regolith for case number 5 in Table 4.2 with direction of SRP and STBE perturbation vectors. Note that the vectors are shown only for those parts of the trajectory where the SRP magnitude is of the same order as that of the asteroid's gravitational acceleration. For those very same points along the trajectory, the magnitude of the STBE is always 1.0 order of magnitude smaller than the gravitational acceleration. Particle code LoGSP-1.



(a)



(b)

Figure 4.10: 2D trajectory of capture regolith for case number 5 in Table 4.2 with direction of the sum total of SRP and STBE perturbation vectors, and the direction of the gravitational acceleration vector for the same data points. Note that the vectors are shown only for those parts of the trajectory where the SRP magnitude is of the same order as that of the asteroid's gravitational acceleration. For those very same points along the trajectory, the magnitude of the STBE is always 1.0 order of magnitude smaller than the gravitational acceleration. Particle code LoGSP-1.

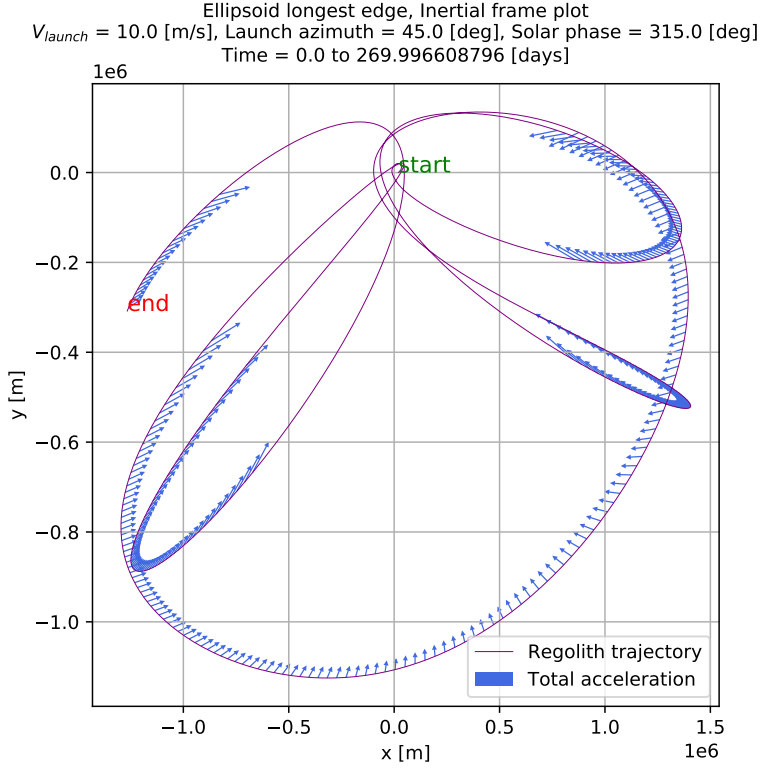


Figure 4.11: 2D trajectory of capture regolith for case number 5 in Table 4.2 with direction of the net acceleration vector. Note that the vectors are shown only for those parts of the trajectory where the SRP magnitude is of the same order as that of the asteroid's gravitational acceleration. For those very same points along the trajectory, the magnitude of the STBE is always 1.0 order of magnitude smaller than the gravitational acceleration. Particle code LoGSP-1.

Both SRP and STBE together are necessary in getting the capture trajectory shown in Figure 4.8. If either one of them is removed from the simulation, for the same launch conditions and initial Solar phase angle, then the results are completely different and we do not get a capture orbit. Note that the definition of capture orbit in this context implies that the particle stays in an orbit around the asteroid for the complete duration of 270.0 [days], i.e., the maximum time for which the simulation is run.

When only STBE is removed, then we get a trajectory where the particle eventually escapes the asteroid. This is shown in Figure 4.12. The trajectory is completely different from the one in Figure 4.8, even though the only difference between the two simulations is the omission of STBE perturbation. Figure 4.13a shows the direction of perturbing acceleration due to SRP and the gravitational acceleration for those points along the trajectory where both have the same order of magnitude. The direction for the net acceleration acting on the particle is shown in Figure 4.13b. The trajectory of the particle starts out the same way in both Figure 4.12 and Figure 4.8 however due to the lack of STBE perturbation, the trajectories soon start to differ from each other. Upon comparing Figure 4.11 and Figure 4.13b we can infer that the trajectories differ because the with the lack of STBE the direction of the net acceleration vector differs for the two trajectories which eventually directs how the particle motion would progress. The particle trajectory in Figure 4.12 eventually leads to an escape scenario. Now if we look at Figure 4.13a, towards the end of the trajectory, the direction of the gravitational vector gradually changes and starts to point along the instantaneous tangent to the trajectory, all the while with the SRP vector pointing away from the asteroid. The net effect of this situation can be seen in Figure 4.13b; we see that the net acceleration vector starts pointing away from the asteroid towards the end segment of the trajectory and thus this is when the particle escapes.

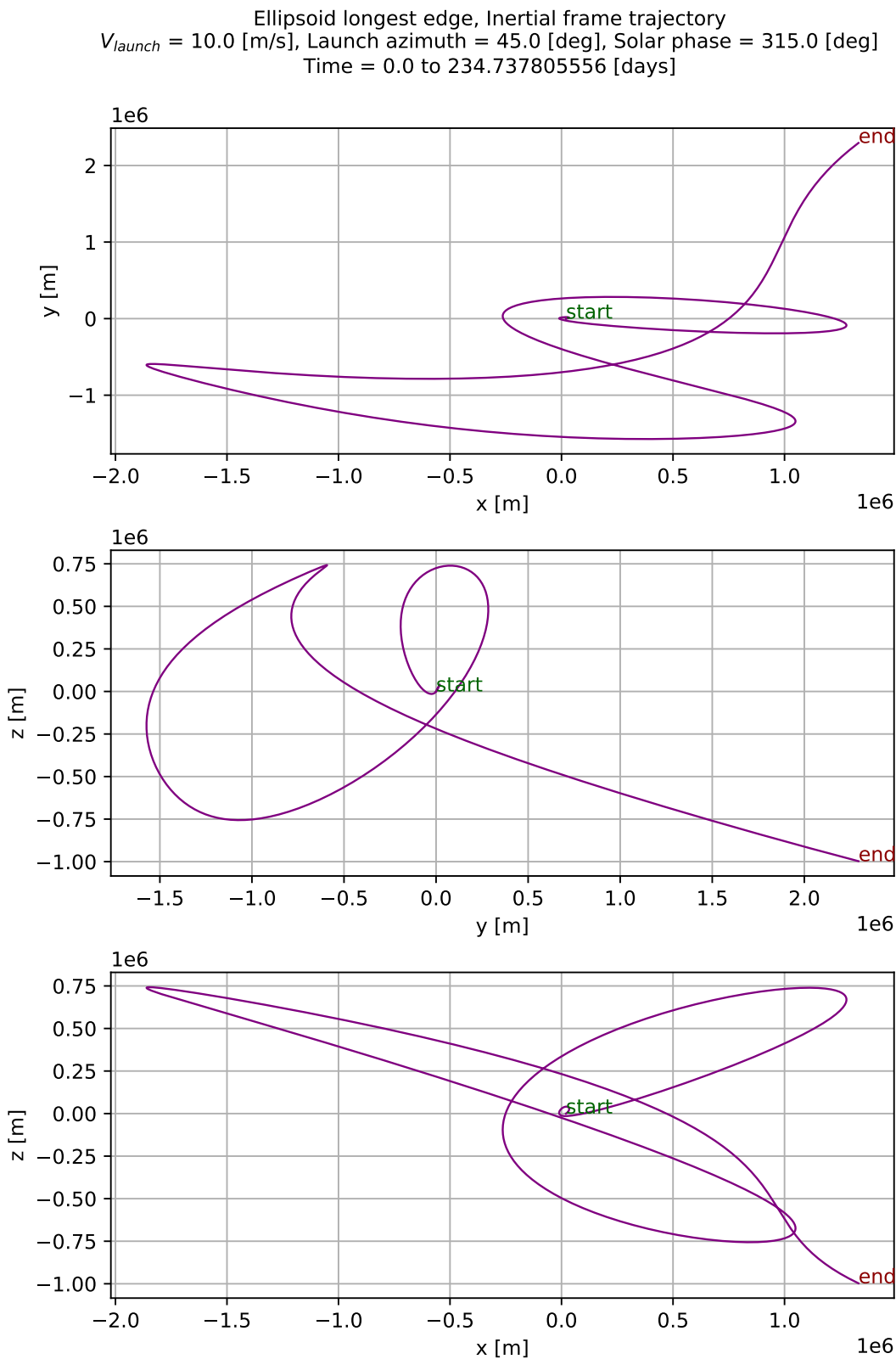
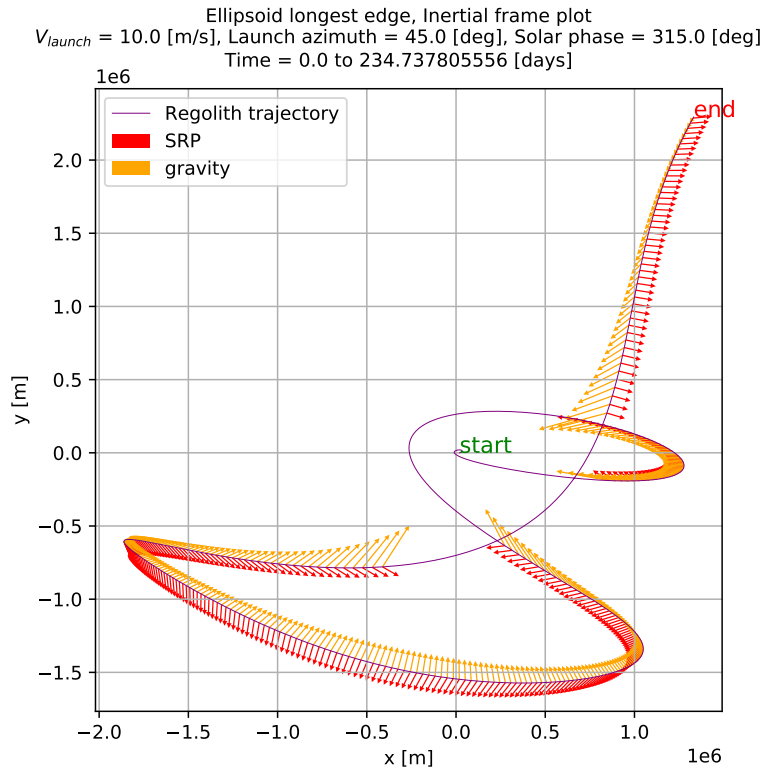
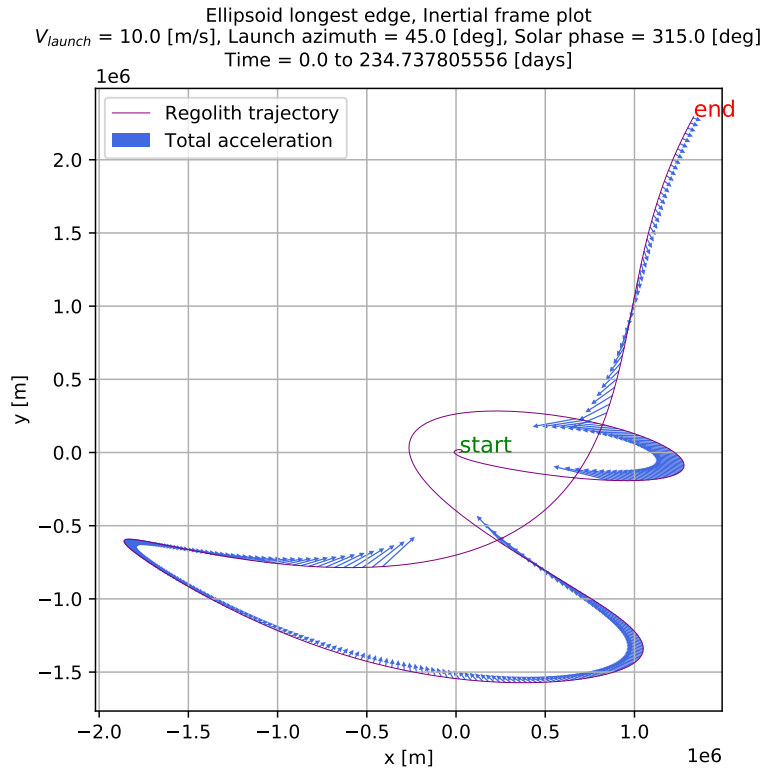


Figure 4.12: 2D trajectory of particle for same initial conditions as that of capture case 5 in Table 4.2 except that only SRP was included in this simulation. Particle code LoGSP-1.



(a)



(b)

Figure 4.13: Inertial frame XY plane trajectory for same launch conditions as that of capture case 5 in Table 4.2: (a) showing direction of SRP acceleration and gravitational acceleration & (b) showing direction of the net acceleration acting on the particle. Vectors are shown only for those parts of trajectory where acceleration due to SRP and gravity have the same order of magnitude. Note that STBE perturbation was not part of the simulation here. Particle code LoGSP-1.

When we keep STBE but remove SRP from our simulations, then the trajectory again leads to an escape situation, only this time its much faster. The 2D inertial frame trajectory is shown in Figure 4.15. The trajectory shows similarity only for a brief moment immediately after launch (notice the small loop after 'start') with the capture case in Figure 4.8 but soon after the particle is on a trajectory that never comes back around the asteroid. The reason for this is clear and simple if one looks at the direction of acceleration due to gravity and STBE in Figure 4.16a and their net effect in Figure 4.16b. Initially, from the point when we show these vectors, we know that the magnitude of STBE acceleration is 1.0 order of magnitude smaller than the gravitational acceleration (see Figure 4.17) and even then the direction of the net acceleration vector is such that the trajectory can not loop around the asteroid. The STBE magnitude increases soon enough to the same order as that of gravitational acceleration and the net acceleration vector direction never points towards the asteroid which eventually causes the particle to escape. However, the point where the magnitude curves of STBE and gravitational acceleration cross is not the point where the escape occurs as is evident from the plot for total energy and eccentricity in Figure 4.14.

From this analysis, we can say that effect of removing SRP from simulations had a much drastic effect than removing just the STBE. Both cases lead to an escape situation and the combined effect of both the perturbations leads to a capture orbit, for the same launch conditions and initial Solar phase angle. The behavior of the trajectory, in all cases, can be easily understood by looking at the direction of the net acceleration vector, especially when the particle is far away from the asteroid because it tells us exactly, how by adding perturbations, the motion of the particle is affected and not just in terms of its final fate but even in terms of changing its orbital direction.

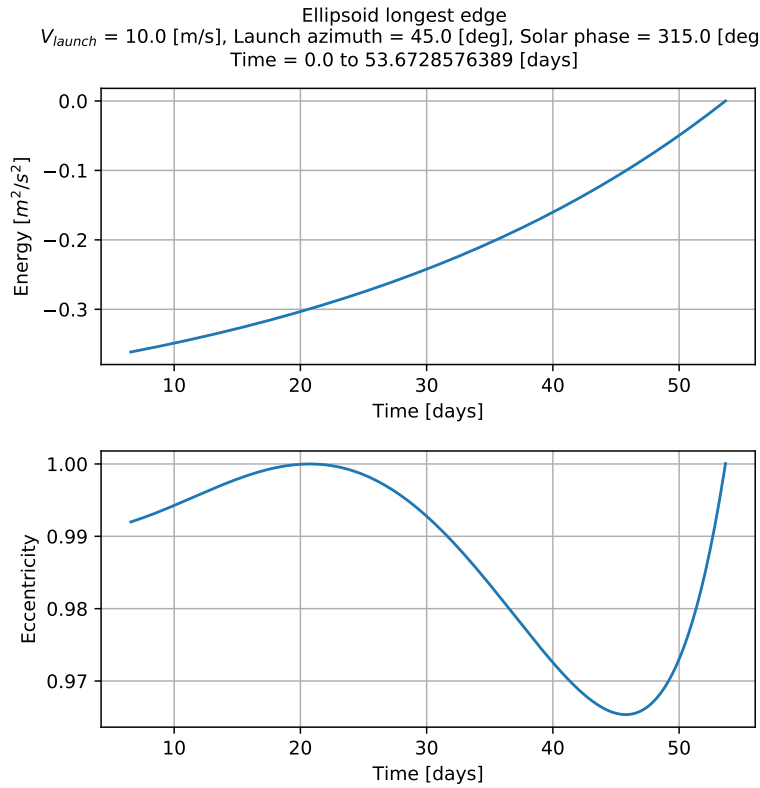


Figure 4.14: Evolution of total energy of the particle and its orbital eccentricity. Particle has the same initial conditions as that of capture case 5 in Table 4.2 except that only STBE was included in this simulation. The range of data points plotted is the same as that in Figure 4.16. Particle code LoGSP-1.

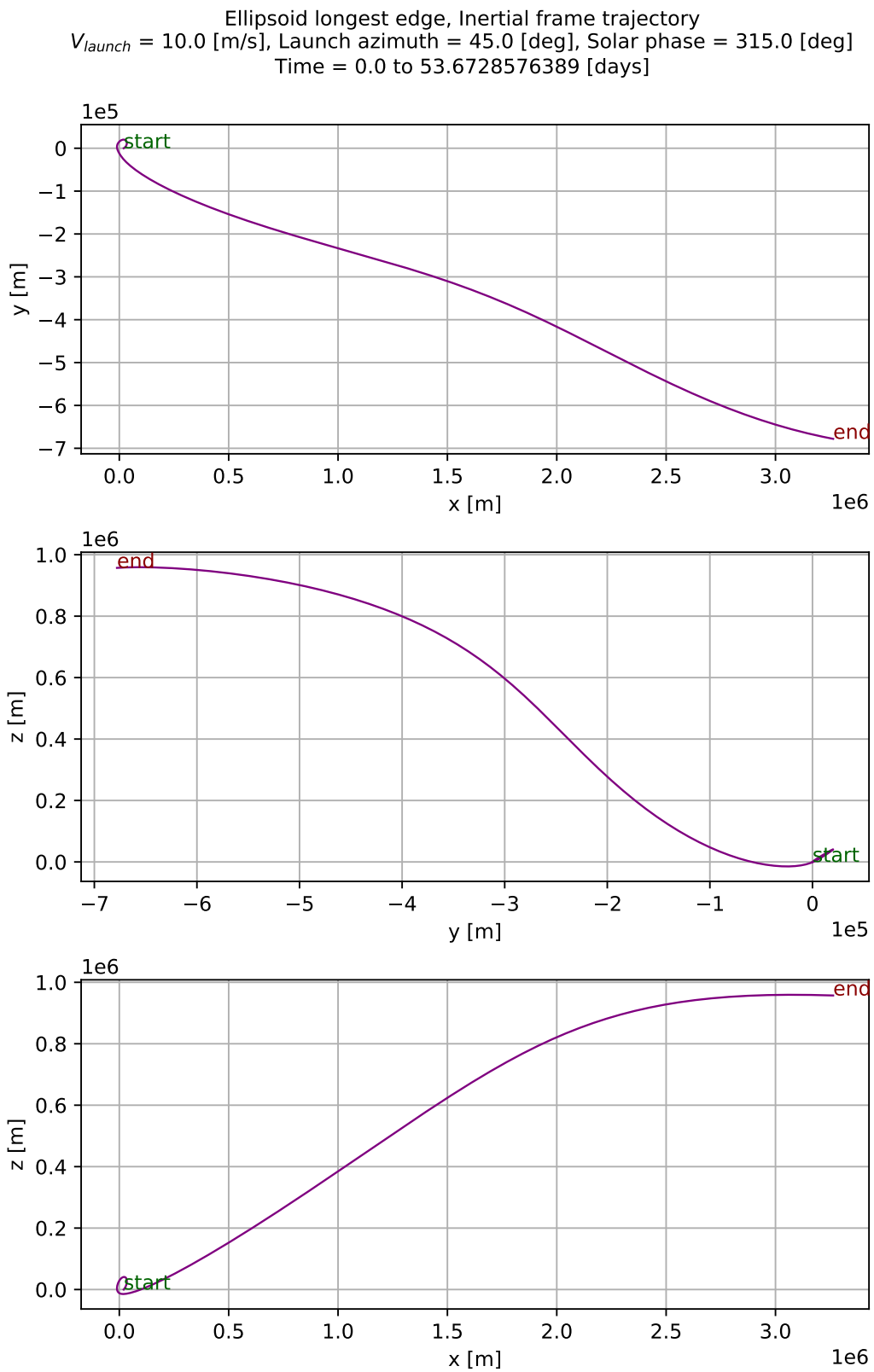
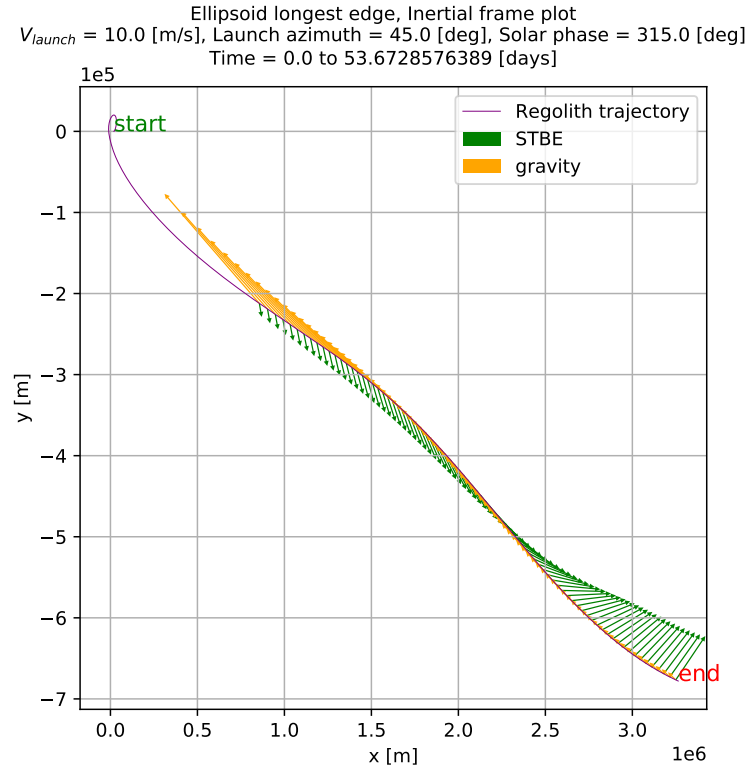
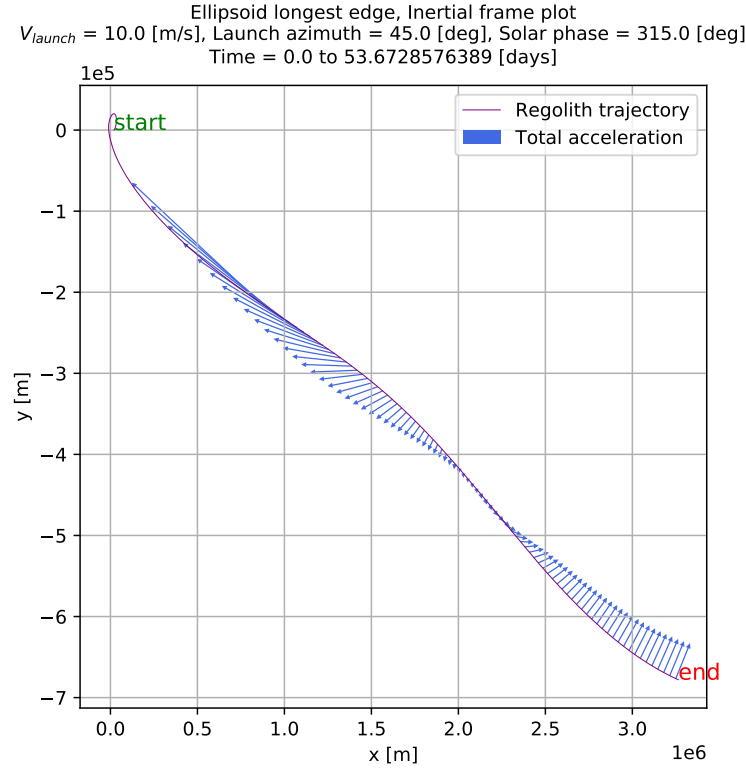


Figure 4.15: 2D trajectory of particle for same initial conditions as that of capture case 5 in Table 4.2 except that only STBE was included in this simulation. Particle code LoGSP-1.



(a)



(b)

Figure 4.16: Inertial frame XY plane trajectory for same launch conditions as that of capture case 5 in Table 4.2: (a) showing direction of STBE acceleration and gravitational acceleration & (b) showing direction of the net acceleration acting on the particle. Vectors are shown only for those parts of trajectory where acceleration due to STBE is equal to gravitational acceleration or smaller than it by 1.0 order of magnitude. Note that SRP perturbation was not part of the simulation here. Particle code LoGSP-1.

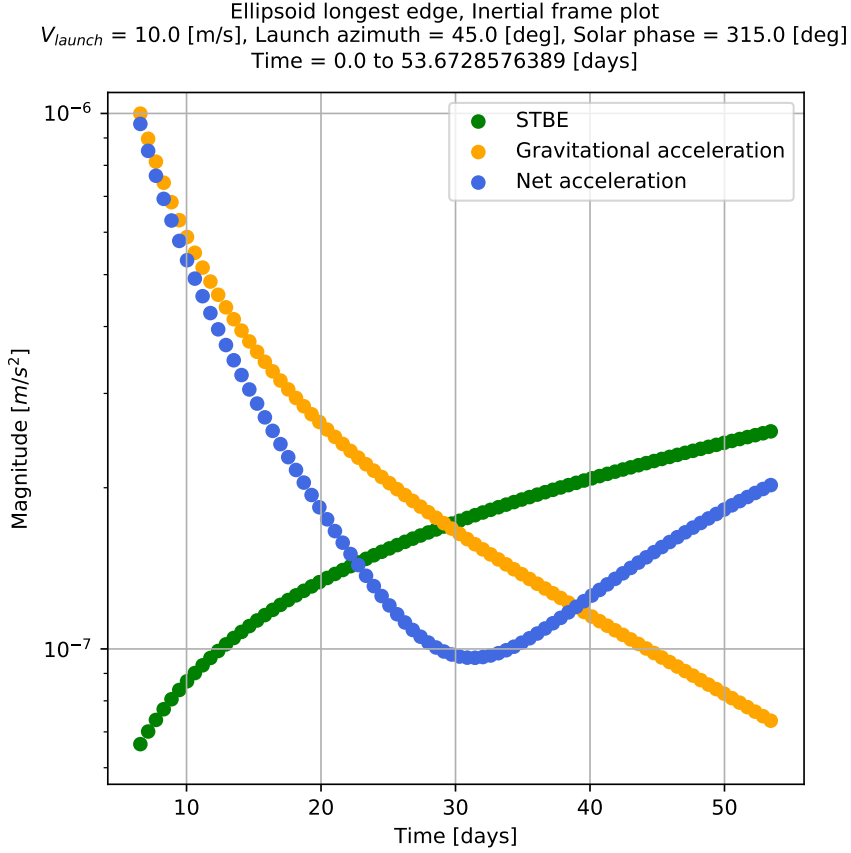
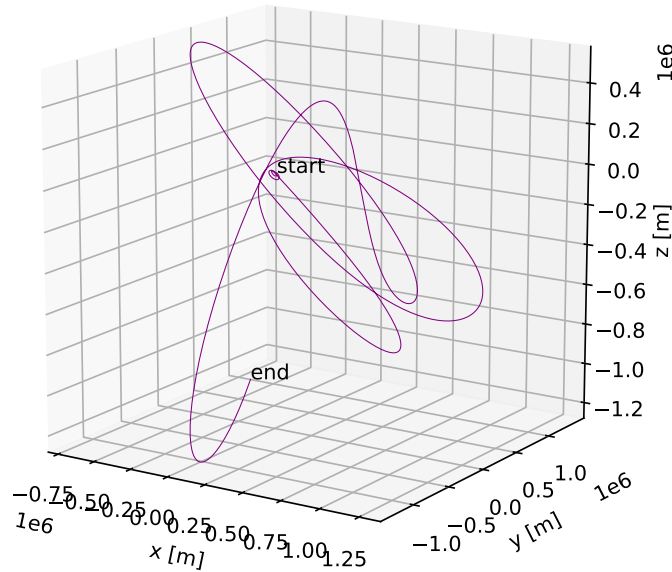


Figure 4.17: Magnitudes of acceleration due to gravity, STBE and the net effect of the two for the corresponding vectors as shown in Figure 4.16. Particle code LoGSP-1.

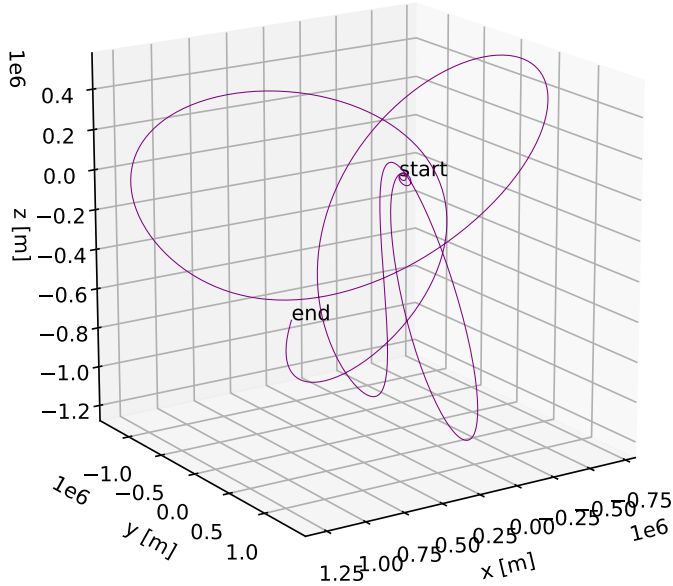
Figure 4.18 shows the 3D trajectory for completely different launch conditions (see capture case 8 in Table 4.2). The 3D trajectory as viewed from the asteroid centric body fixed frame is shown in Figure A.4. The 2D trajectory projections for the same, in inertial and body fixed frames, are shown in Figure 4.19 and Figure A.5 respectively. Just like in the previous case, we see from the animation (see Figure 4.23) and the 3D trajectory for current launch conditions, that the particle direction of motion is reversed twice in its course. These two locations are marked by numbers 1 and 2 in Figure 4.19. At location number 1 we see that the motion changes from anti-clockwise to clockwise direction in the XY plane. The case for location number 2 is exactly the opposite. If we look at Figure 4.21a, the change in direction of motion is consistent with the direction in which the net perturbing force is acting. Ultimately, when we look at the net acceleration acting on the particle in Figure 4.22, we can understand how exactly the particle would orbit around the asteroid. The net force, gravitational and perturbations combined, act in a direction such that the particle is forced to change its orbital motion direction at the two locations previously explained. The acceleration vectors in Figures 4.20 to 4.22 are plotted for points along the trajectory where the magnitude of acceleration due to SRP is of the same order of magnitude as the gravitational acceleration. Again, the magnitude of STBE is 1.0 order of magnitude smaller than the gravitational acceleration for the same data points along the trajectory.

Ellipsoid longest edge, Inertial frame trajectory
 $V_{\text{launch}} = 8.0 \text{ [m/s]}$, Launch azimuth = 165.0 [deg], Solar phase = 45.0 [deg]
 Time = 0.0 to 270.0 [days]



(a)

Ellipsoid longest edge, Inertial frame trajectory
 $V_{\text{launch}} = 8.0 \text{ [m/s]}$, Launch azimuth = 165.0 [deg], Solar phase = 45.0 [deg]
 Time = 0.0 to 270.0 [days]



(b)

Figure 4.18: 3D inertial frame trajectory of capture regolith for case number 8 in Table 4.2 from two different viewing angles. Particle code LoGSP-1.

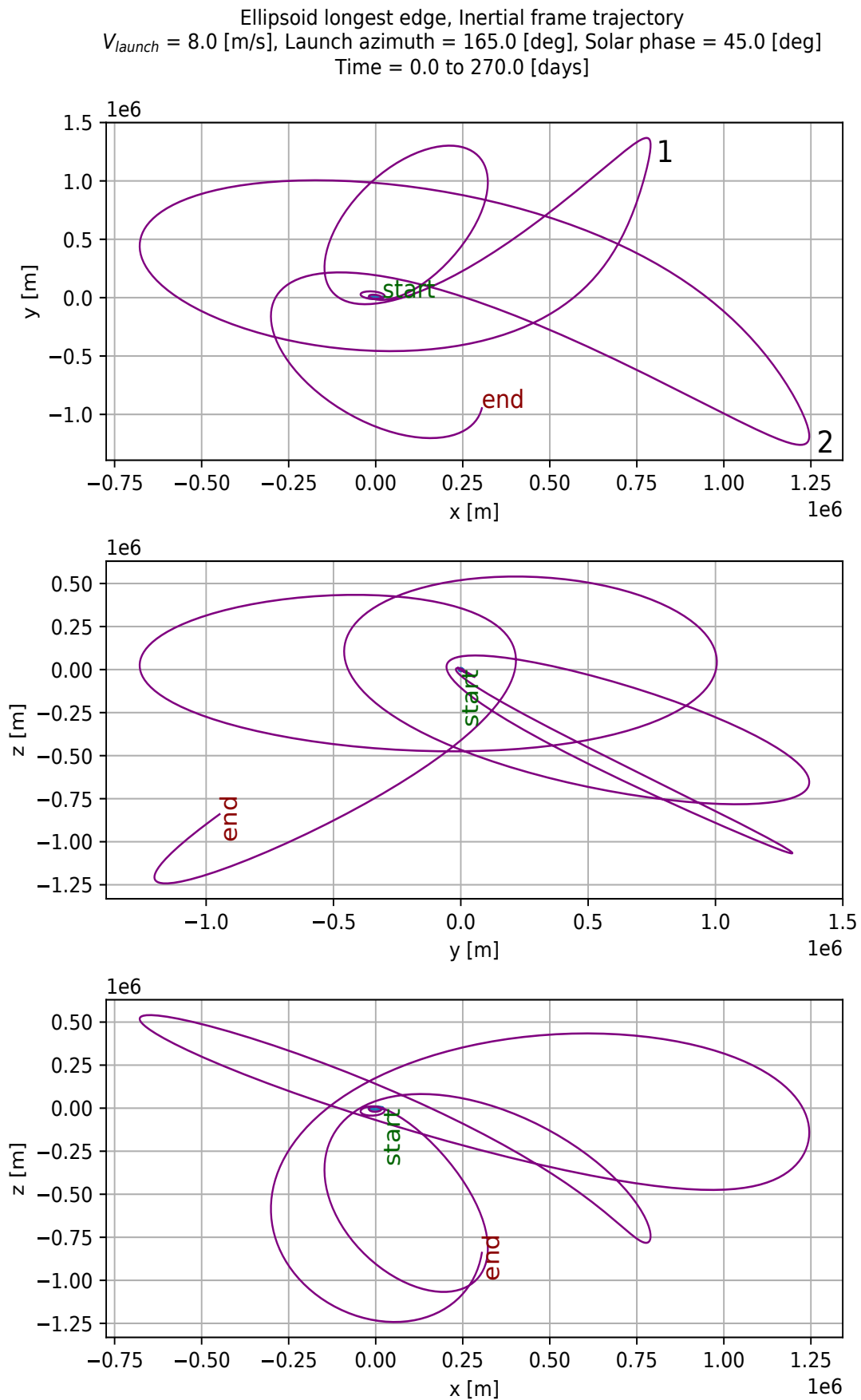
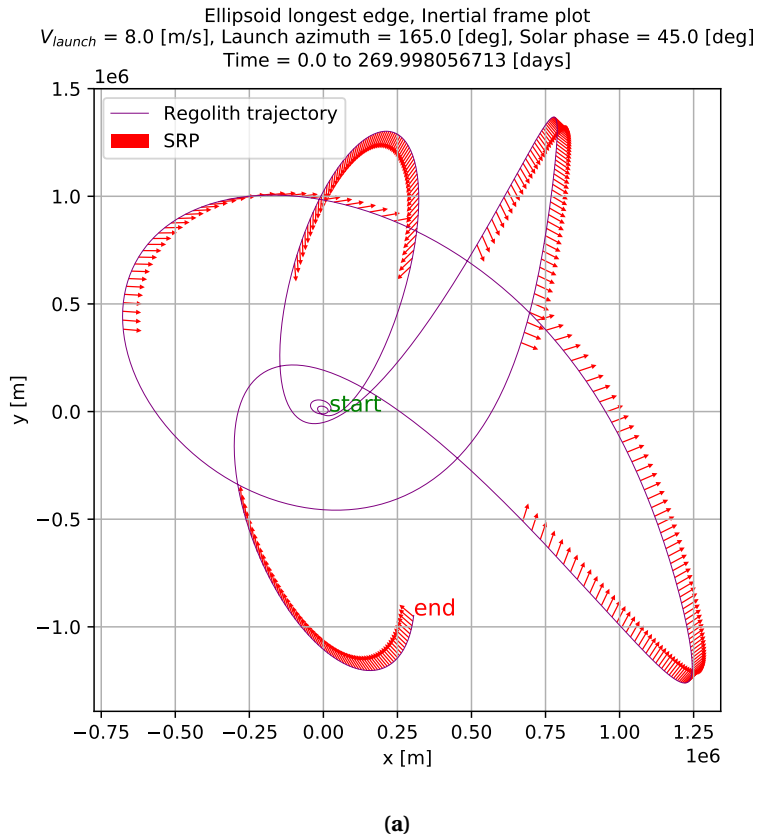
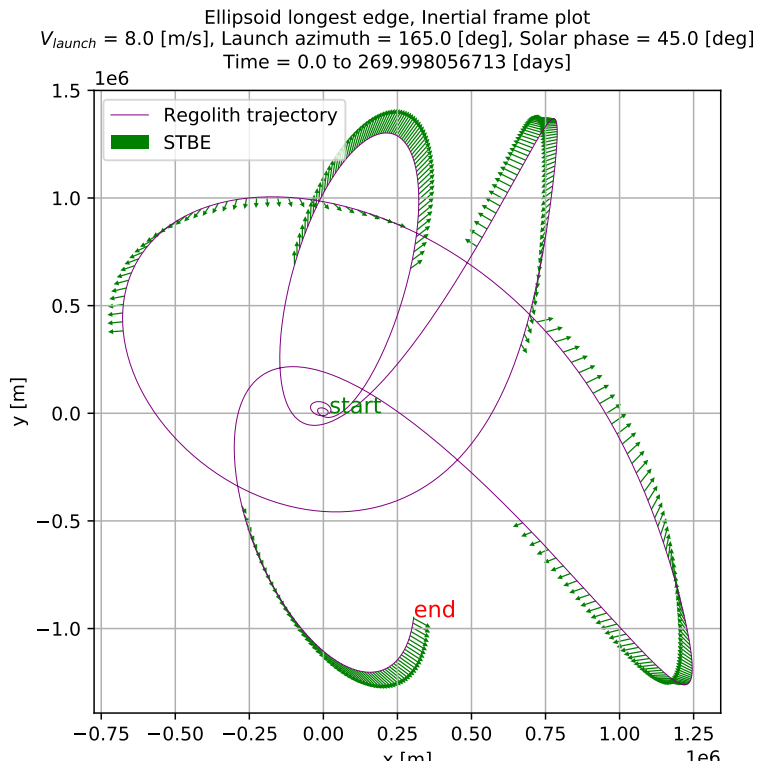


Figure 4.19: 2D inertial frame trajectory of capture regolith for case number 8 in Table 4.2. Particle code LoGSP-1.

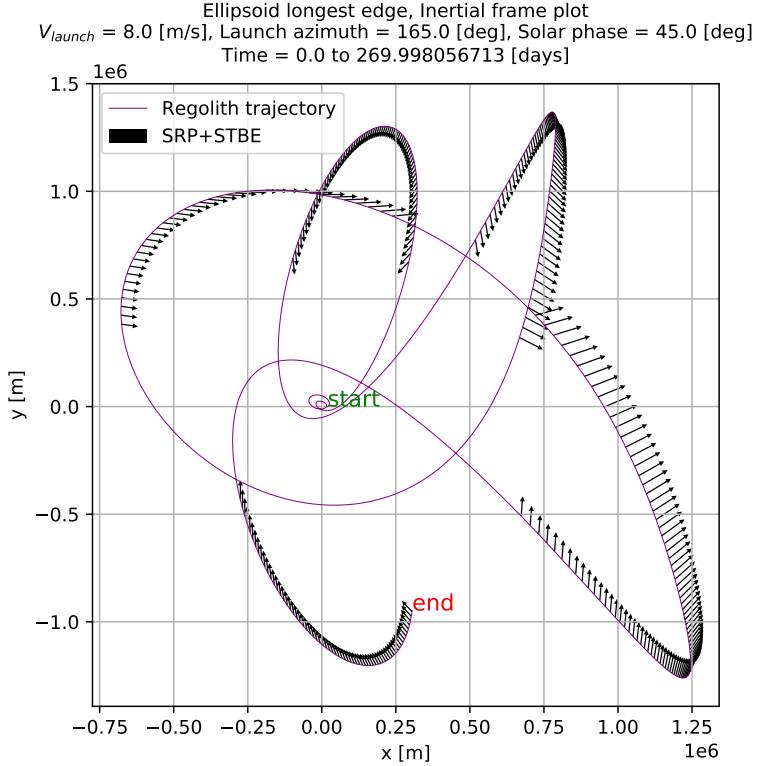


(a)

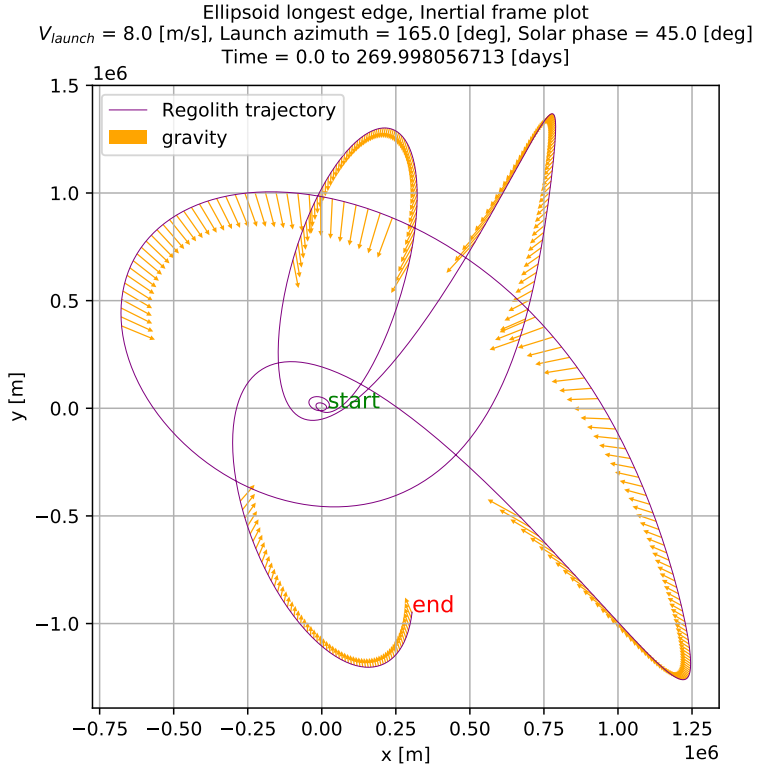


(b)

Figure 4.20: 2D trajectory of capture regolith for case number 8 in Table 4.2 with direction of SRP and STBE perturbation vectors. Note that the vectors are shown only for those parts of the trajectory where the SRP magnitude is of the same order as that of the asteroid's gravitational acceleration. For those very same points along the trajectory, the magnitude of the STBE is always 1.0 order of magnitude smaller than the gravitational acceleration. Particle code LoGSP-1.



(a)



(b)

Figure 4.21: 2D trajectory of capture regolith for case number 8 in Table 4.2 with direction of the sum total of SRP and STBE perturbation vectors, and the direction of the gravitational acceleration vector for the same data points. Note that the vectors are shown only for those parts of the trajectory where the SRP magnitude is of the same order as that of the asteroid's gravitational acceleration. For those very same points along the trajectory, the magnitude of the STBE is always 1.0 order of magnitude smaller than the gravitational acceleration. Particle code LoGSP-1.

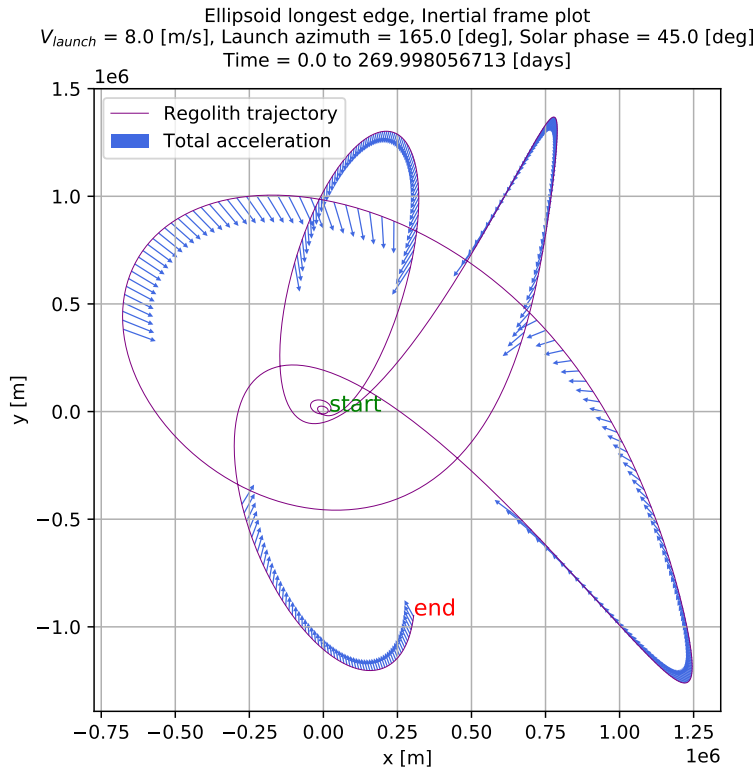


Figure 4.22: 2D trajectory of capture regolith for case number 8 in Table 4.2 with direction of the net acceleration vector. Note that the vectors are shown only for those parts of the trajectory where the SRP magnitude is of the same order as that of the asteroid's gravitational acceleration. For those very same points along the trajectory, the magnitude of the STBE is always 1.0 order of magnitude smaller than the gravitational acceleration. Particle code LoGSP-1.



Figure 4.23: 2D trajectory animation (XY Plane) of capture regolith for case number 8 in Table 4.2. Particle code LoGSP-1. Scan the QR code to view the animation or use the following web-link: <https://youtu.be/CceYR1NvAim>

We saw in the analysis of capture case number 5 for particle LoGSP-1 that both SRP and STBE were necessary for getting that specific capture trajectory and removal of either of the perturbations resulted in a different final fate for the same particle. The next analysis that we present now, will tell us about how a capture scenario occurs, relative to a situation when all perturbations are removed, for the same initial launch conditions in both cases. We do the analysis for capture case number 8 from Table 4.2. Figure 4.25a shows two different trajectories for the particle launched with the same initial conditions. The one shown in dotted line is for the case when Solar perturbations were omitted from the simulation, which eventually results in the particle escaping the asteroid after 1.4 [days]. The one in the solid line shows the capture trajectory (actually a section of the entire capture trajectory as seen in Figure 4.19) when Solar perturbations were included in the simulation. Note that we show the perturbed trajectory (capture case) for the same amount of time (1.4 [days] instead of 270.0 [days]) as taken by the unperturbed trajectory (escape case) to be able to do a one-to-one comparison. The arrows plotted along this trajectory indicate the direction of the net perturbing

acceleration due to SRP and STBE. Figure 4.24 directs to an animation for both the unperturbed and perturbed trajectory.

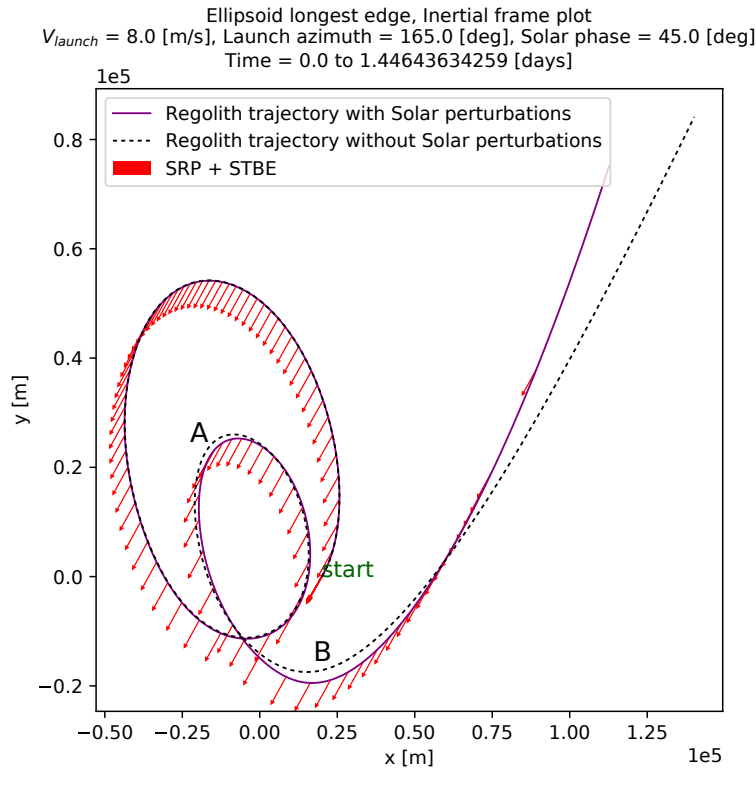


Figure 4.24: 2D trajectory animation (XY Plane) of capture regolith for case number 8 in Table 4.2, compared with that of its unperturbed counterpart. Particle code LoGSP-1. Scan the QR code to view the animation or use the following web-link: <https://youtu.be/CdFKKR3UDJ0>

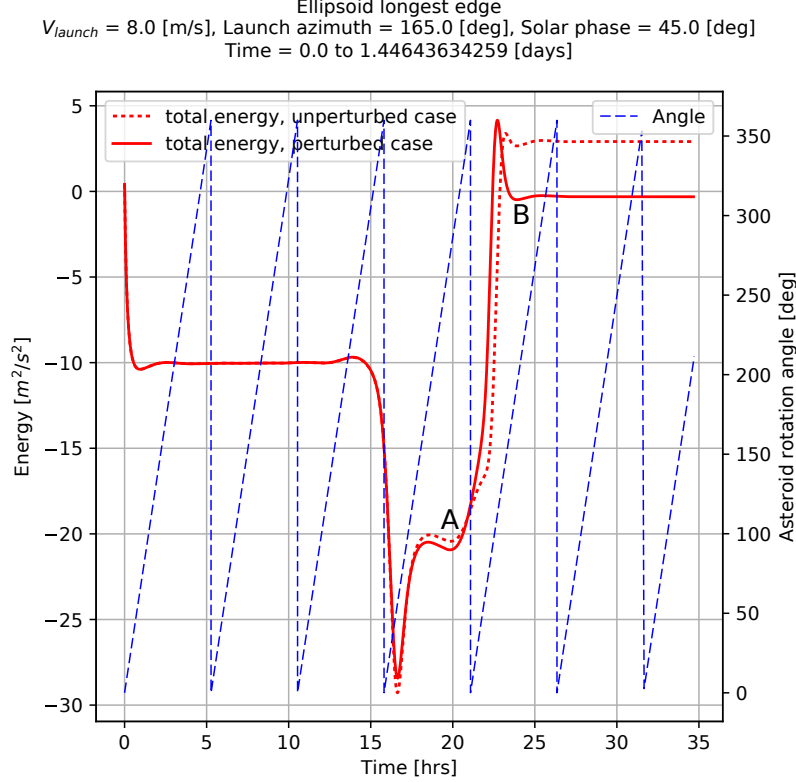
From the animation we can see that even as the particle has just been lofted from the surface of the asteroid, there are very subtle and minute differences in the range to the particle and its velocity, between the perturbed and unperturbed trajectory. The first visible difference between the two trajectories becomes noticeable at point "A" in Figure 4.25a. It is easy to deduce the change in the perturbed trajectory from the direction of the net perturbing acceleration up until this point. The same point "A" is also marked in Figure 4.25b. It is from this point that we can see noticeable difference between the two trajectories as well as in their corresponding energies. A snippet from the trajectory animation, corresponding to the point "A", is shown in Figure 4.29a which highlights the differences in range and velocity of the particles in the two trajectories. Note that in Figure 4.29a, the difference in the velocity between the perturbed and unperturbed cases is relatively small, compared to almost 1 [km] of a difference in range of the particles. The latter is significant since the particles have dimensions in the order of [cm]. From point "A" onwards these differences continue to grow and only get larger as the trajectory proceeds.

Similarly, at point "B" in Figure 4.25a, we see a much larger difference in the two trajectories. In Figure 4.25b, we see that around point "B" both trajectories have a positive energy which quickly comes down to a negative value for the perturbed trajectory, hence keeping it bounded which results in a capture scenario. However, this does not happen for the unperturbed trajectory, leading to an escape scenario. The difference in the state of the two particles at point "B" are relatively larger and can be seen in Figure 4.29b. The differences in the two trajectories, computed in the asteroid centric rotating frame, is shown in Figure 4.26. The plot on the bottom shows the trajectory for 1.4 [days] (i.e. until escape for the unperturbed trajectory) as viewed in the rotating frame, and the plot on the right zooms into a small part of this trajectory to show how Solar perturbations are responsible for changing the course of the particle. It is seen with a bit more clarity on how the net perturbation vector pulls the trajectory away from the trace of the unperturbed one.

So what we are seeing here is, that due to the inclusion of perturbations from the Sun, the motion of the particle changed from its unperturbed counterpart. This change was not drastic in terms of the initial shape of the trajectory as seen in Figure 4.25a. But the change was just enough for the particle to have a different phase with respect to the asteroid, relative to the unperturbed trajectory as seen in Figure 4.29. By phase, we refer to the location of the particle with respect to a given rotational state of the asteroid. So if two particles are at different locations, at any given epoch and for the same rotational state of the asteroid, they will have different magnitudes of forces acting on them which would ultimately lead to different final outcomes.



(a)



(b)

Figure 4.25: Comparative analysis of capture case 8 in Table 4.2 with a particle trajectory where the initial conditions are same as the former but the simulation was done without Solar perturbations. Figure 4.25a compares the XY plane trajectory & Figure 4.25b compares their total energy. Particle code LoGSP-1.

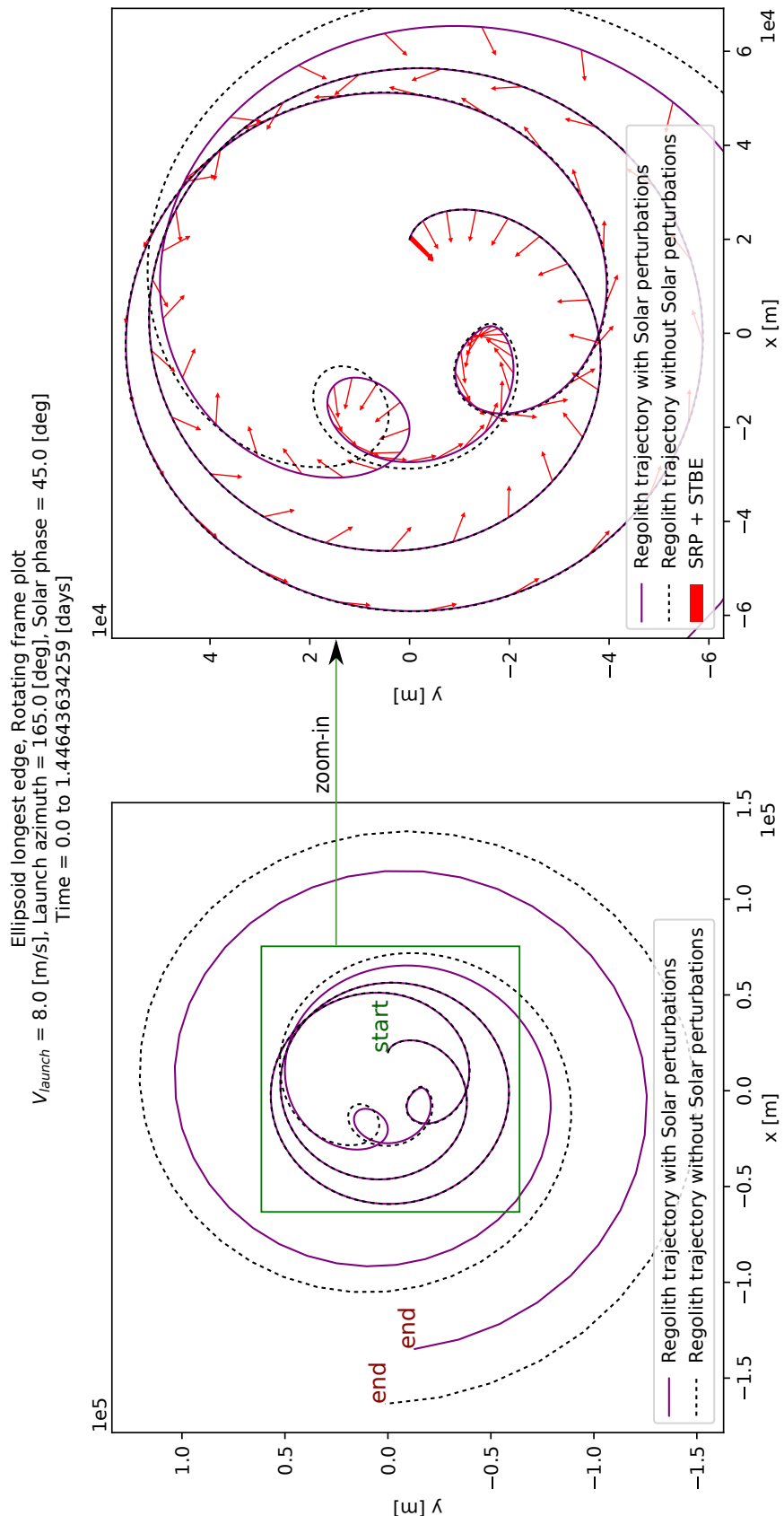


Figure 4.26: Rotating frame 2D trajectory (XY plane) of capture regolith for case number 8 in Table 4.2 with direction of the net perturbation vector, compared with the trajectory of a particle launched with the same initial conditions but in absence of Solar perturbations. Particle code LoGSP-1.

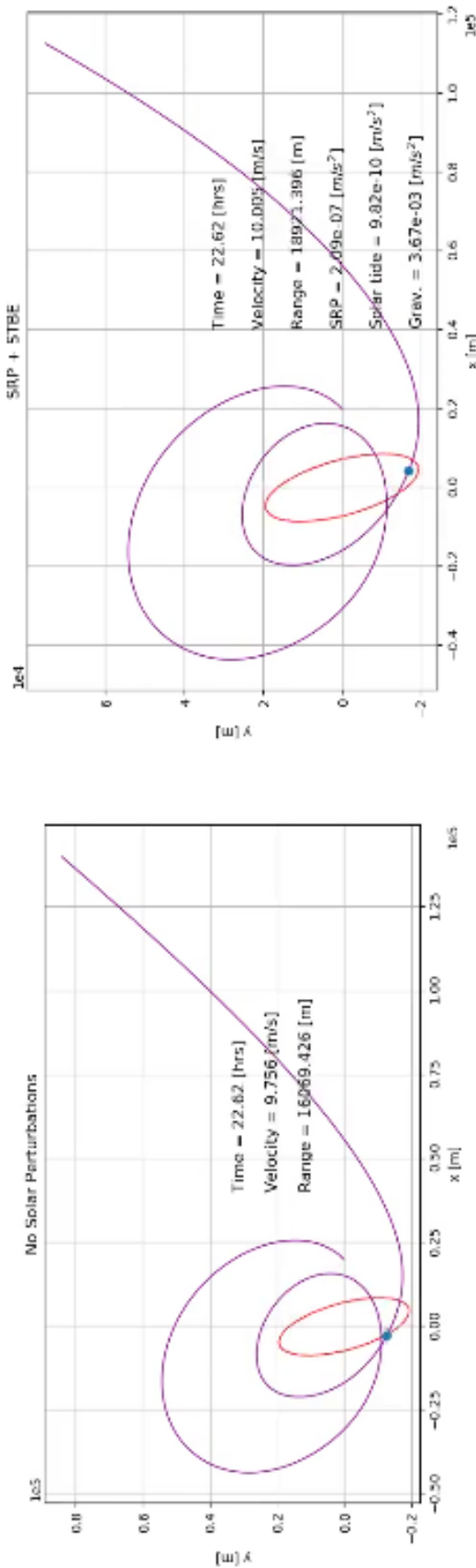


Figure 4.27: Snapshot from animation of the perturbed trajectory of capture case 8 in Table 4.2 compared with that of its unperturbed counterpart. The unperturbed trajectory is still being accelerated at the given instant however the particle in the perturbed trajectory is being decelerated. Particle code LoGSP-1.

If we look at the trajectory animation in Figure 4.24, one would notice that at around point "B", the particle in the unperturbed trajectory is being accelerated by the gravitational pull of the asteroid while the particle in the perturbed trajectory is being slowed down. A snapshot of this scenario from the animation is shown in Figure 4.27. Although this situation does not happen for extended periods of time, but only while approaching point "B", we see that the particle in the unperturbed trajectory has relatively higher velocity while moving forth of point "B" and leaving the vicinity of the asteroid, relative to the particle in the perturbed trajectory. The latter thus stays in a capture orbit while the former has enough velocity to escape. A plot for this is shown in Figure 4.28.

Note that in the capture case just discussed, the magnitude of the perturbing accelerations is much smaller than the gravitational acceleration. The effect of the perturbations on the particle's trajectory is not instantaneous and we can see that in the initial part of the trajectories up until point "A" in Figure 4.25a. Until this point, acceleration due to gravity is in the order of 10^{-4} , while accelerations due to SRP and STBE are in the orders of 10^{-7} and 10^{-9} respectively. Although the perturbing magnitudes are small, but the particles in question are extremely small as well and so over time, the perturbing accelerations add up, leading to a significant change in the trajectory from the unperturbed one.

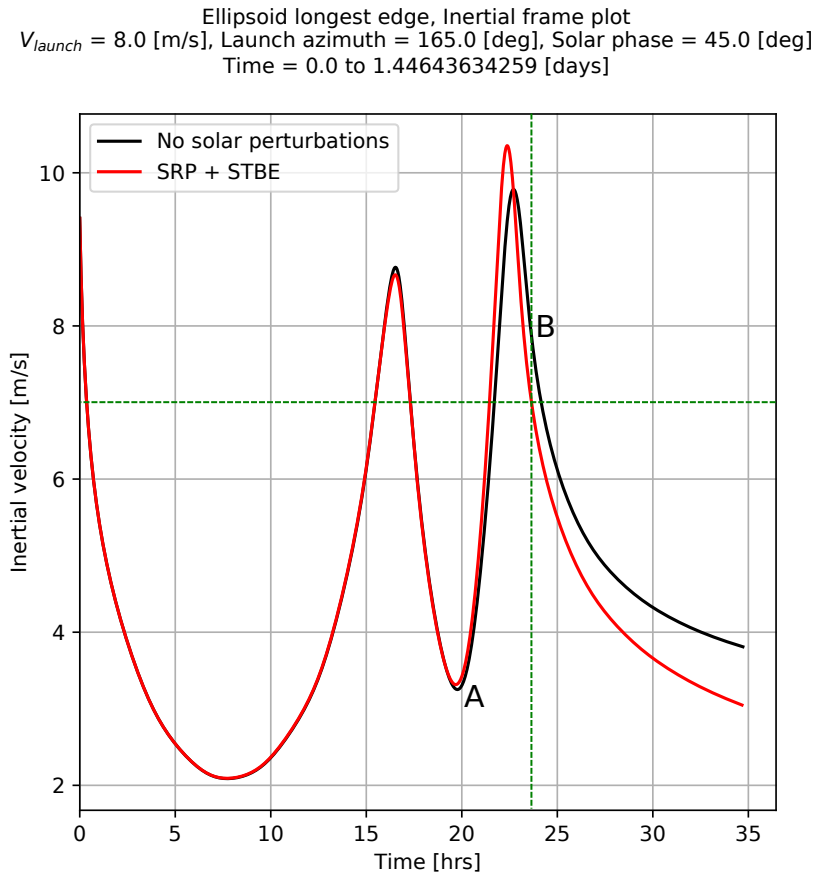


Figure 4.28: Inertial velocity of the perturbed trajectory of capture case 8 in Table 4.2 compared with that of its unperturbed counterpart. The trajectories are shown for the time it takes for the particle in the unperturbed trajectory to escape. Particle code LoGSP-1.

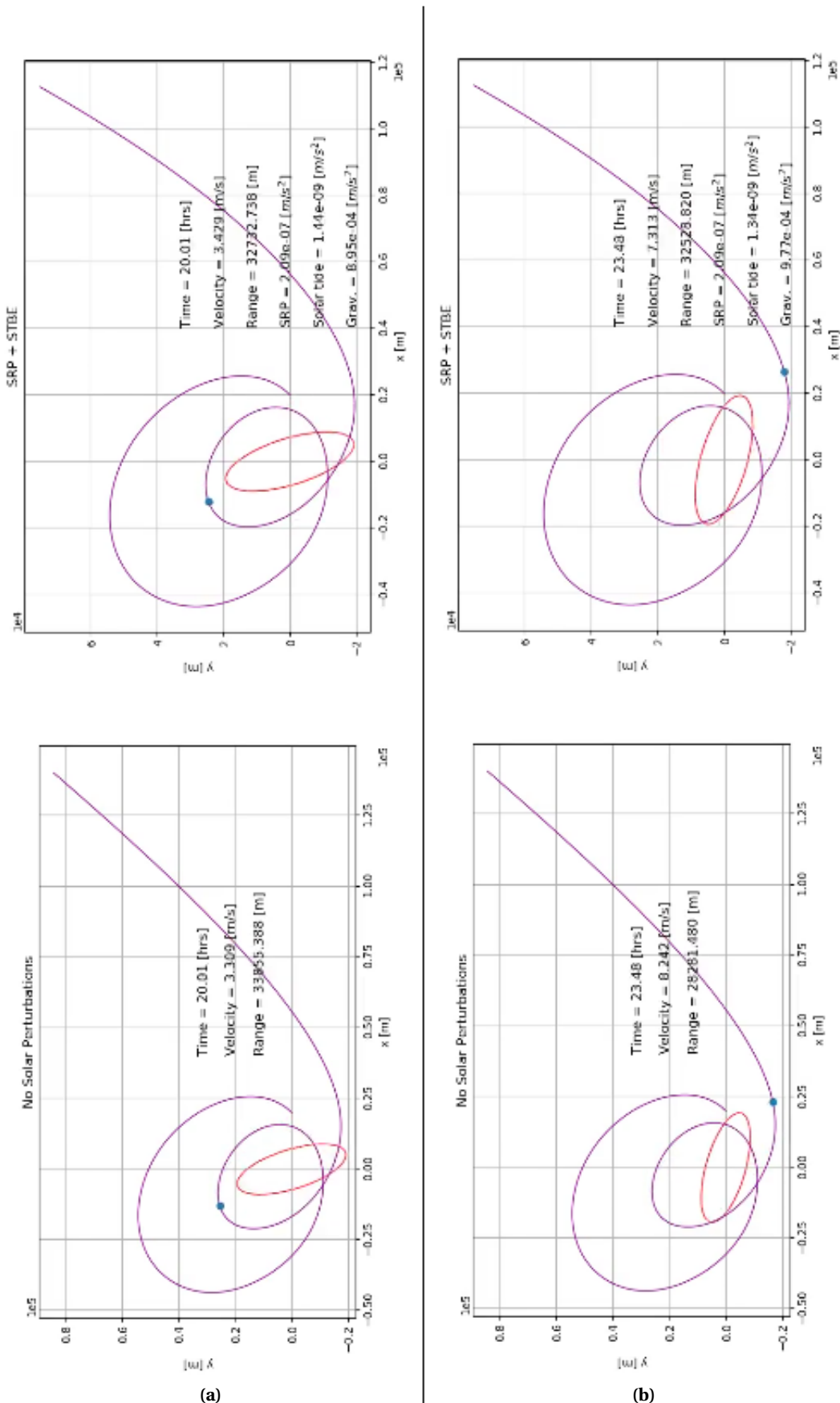


Figure 4.29: Animation snippets of the inertial frame 2D trajectory (XY plane) of capture regolith for case number 8 in Table 4.2. The bottom two plots are for the case when Solar perturbations were omitted from the simulation and the top two plots includes them. Note the differences in the range to the particle and its velocity for the same time stamp and rotational state of the asteroid. Particle code LoGSP-1.

We see a similar effect when we look at capture case number 5 from Table 4.2. The inertial frame trajectory, both perturbed and unperturbed, for it are shown in Figure 4.30. With Solar perturbations removed from the simulation, the initial conditions for this particle result in it getting launched on a highly elliptical orbit and eventually crashing onto the surface of the asteroid after 96 days. The particle, however, avoids this fate when Solar perturbations are included in the simulation. In Figure 4.30, it can be clearly seen that the direction of the perturbing acceleration due to SRP and STBE is consistent with how the trajectory departs from its unperturbed counterpart. The trajectories are shown only for the time it takes for the particle in the unperturbed trajectory to re-impact the surface of the asteroid. We show this case to highlight the effect perturbations have on a trajectory destined for re-impact, unlike the escape scenario discussed previously. We see drastic changes in the perturbed trajectory from the unperturbed one because when the particle is far away from the asteroid, the perturbing acceleration magnitude is of the same order as that of the gravitational acceleration.

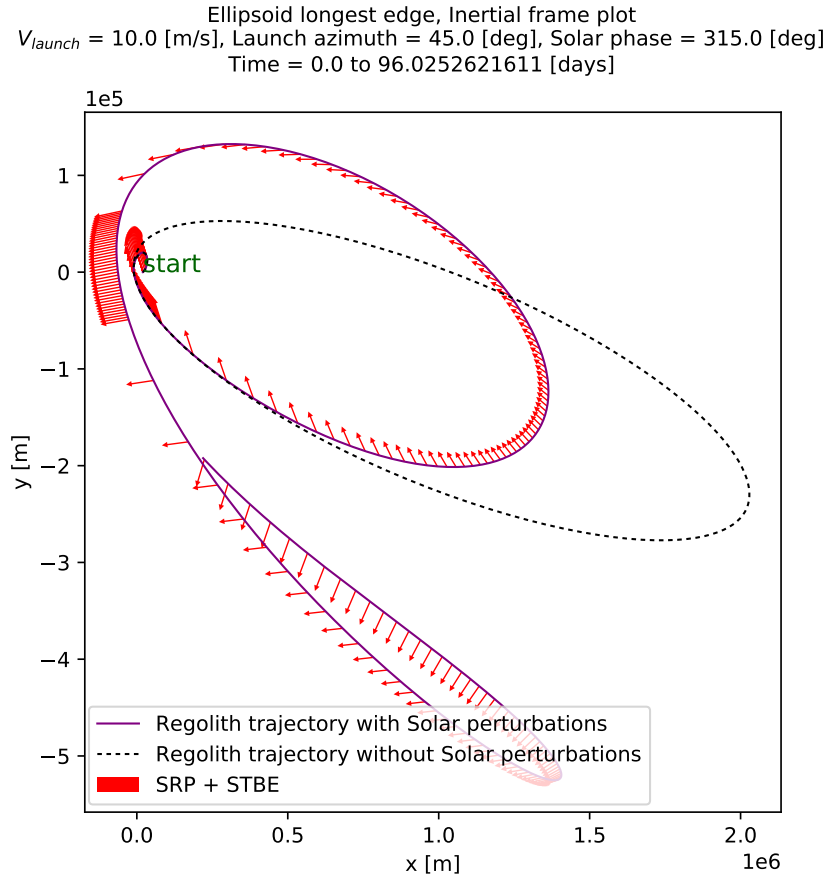


Figure 4.30: Inertial frame 2D trajectory (XY plane) of capture regolith for case number 5 in Table 4.2 with direction of SRP perturbation vector compared with the trajectory of a particle launched with the same initial conditions but in absence of Solar perturbations. Trajectories shown for as long as it takes the unperturbed trajectory Particle code LoGSP-1.

FINAL FATE BEHAVIOR OF DIFFERENT REGOLITH TYPES

For simulations accounting Solar perturbations, the discussion so far has been about how perturbations affect particle motion and specifically the capture scenario, relative to a particle in an unperturbed simulation. We did this detailed analysis for a single particle type only, namely LoGSP-1 from Table 4.1. We shall now look into the final fate behavior of all the regolith types mentioned in

Table 4.1 to understand how particle motion is affected for different densities and sizes. The simulations were conducted one-by-one for each regolith type, in the same manner as described earlier for particle LoGSP-1. All particles were launched from the longest edge of the asteroid.

BIBLIOGRAPHY

- Berry, Kevin et al. (2013). "OSIRIS-REx touch-and-go (TAG) mission design and analysis". In: Biele, Jens and Ulamec, Stephan (2008). "Capabilities of Philae, the Rosetta lander". In: *Space Science Reviews* 138.1, pp. 275–289.
- Bottke, William Frederick (2002). *Asteroids III*. University of Arizona Press.
- Cunningham, Clifford (2016). *The Discovery of Ceres*. Springer, pp. 25–39.
- De Pater, Imke and Lissauer, Jack J (2015). *Planetary sciences*. Cambridge University Press.
- ESA (European Space Agency) (2014). *Missions To Asteroids*. Accessed 31 October 2017. URL: <http://sci.esa.int/rosetta/54342-missions-to-asteroids/>.
- Evans, Larry G et al. (2001). "Elemental composition from gamma-ray spectroscopy of the NEAR-Shoemaker landing site on 433 Eros". In: *Meteoritics & Planetary Science* 36.12, pp. 1639–1660.
- Fujiiwara, Akira et al. (2006). "The rubble-pile asteroid Itokawa as observed by Hayabusa". In: *Science* 312.5778, pp. 1330–1334.
- Garcia-Yarnoz, Daniel, Sanchez Cuartielles, Joan-Pau, and McInnes, Colin R (2014). "Passive sorting of asteroid material using solar radiation pressure". In: *Journal of Guidance, Control, and Dynamics* 37.4, pp. 1223–1235.
- JPL (Jet Propulsion Laboratory). *SSD (Solar System Dynamics)*. Accessed 17 November 2017. URL: <http://ssd.jpl.nasa.gov>.
- Kargel, Jeffrey S (1994). "Metalliferous asteroids as potential sources of precious metals". In: *Journal of Geophysical Research: Planets* 99.E10, pp. 21129–21141.
- Kawaguchi, Jun'ichiro, Fujiwara, Akira, and Uesugi, Tono (2003). "Hayabusa (MUSES-C)—rendezvous and proximity operation". In: *56th International Astronautical Congress*.
- Keller, Lindsay P and Berger, Eve L (2014). "A Transmission Electron Microscope Investigation of Space Weathering Effects in Hayabusa Samples". In:
- Korycansky, DG and Asphaug, Erik (2004). "Simulations of impact ejecta and regolith accumulation on Asteroid Eros". In: *Icarus* 171.1, pp. 110–119.
- Kubota, Takashi et al. (2006). "Touchdown dynamics for sampling in hayabusa mission". In: *Proceedings of AIAA/AAS Astrodynamics Specialist Conference and Exhibit 2006*.
- Lauretta, Dante S and Team, OSIRIS-Rex (2012). "An overview of the OSIRIS-REx asteroid sample return mission". In: *Lunar and Planetary Science Conference*. Vol. 43.
- Lee, Pascal (1996). "Dust levitation on asteroids". In: *Icarus* 124.1, pp. 181–194.
- McCoy, TJ et al. (2001). "The composition of 433 Eros: A mineralogical—chemical synthesis". In: *Meteoritics & Planetary Science* 36.12, pp. 1661–1672.
- Miller, James K et al. (2002). "Determination of shape, gravity, and rotational state of asteroid 433 Eros". In: *Icarus* 155.1, pp. 3–17.
- Miyamoto, H et al. (2006). "Regolith on a tiny asteroid: Granular materials partly cover the surface of Itokawa". In: *37th Annual Lunar and Planetary Science Conference*. Vol. 37.
- Morbidelli, Alessandro et al. (2000). "Source regions and timescales for the delivery of water to the Earth". In: *Meteoritics & Planetary Science* 35.6, pp. 1309–1320.
- NASA (National Aeronautics and Space Administration). *Asteroids: In depth*. Accessed 17 November 2017. URL: <https://solarsystem.nasa.gov/planets/asteroids/indepth>.
- SKG (Strategic Knowledge Gaps). Accessed 20 November 2017. URL: <https://www.nasa.gov/exploration/library/skg.html>.

- Nittler, Larry R et al. (2001). "X-ray fluorescence measurements of the surface elemental composition of asteroid 433 Eros". In: *Meteoritics & Planetary Science* 36.12, pp. 1673–1695.
- Prockter, L et al. (2002). "The NEAR Shoemaker mission to asteroid 433 Eros". In: *Acta Astronautica* 51.1, pp. 491–500.
- Richter, K and Keller, HU (1995). "On the stability of dust particle orbits around cometary nuclei". In: *Icarus* 114.2, pp. 355–371.
- Robinson, MS et al. (2001). "The nature of ponded deposits on Eros". In: *Nature* 413.6854, pp. 396–400.
- Scheeres, Daniel J (2016). *Orbital motion in strongly perturbed environments: Applications to asteroid, comet and planetary satellite orbiters*. Springer.
- Scheeres, Daniel J et al. (1996). "Orbits close to asteroid 4769 Castalia". In: *Icarus* 121.1, pp. 67–87.
- Scheeres, DJ and Marzari, F (2000). "Temporary orbital capture of ejecta from comets and asteroids: Application to the Deep Impact experiment". In: *Astronomy and Astrophysics* 356, pp. 747–756.
- Tsuda, Yuichi et al. (2013). "System design of the Hayabusa 2—Asteroid sample return mission to 1999 JU3". In: *Acta Astronautica* 91, pp. 356–362.
- Verka, J et al. (2001a). "Imaging of small-scale features on 433 Eros from NEAR: Evidence for a complex regolith". In: *Science* 292.5516, pp. 484–488.
- Verka, J et al. (2001b). "The landing of the NEAR-Shoemaker spacecraft on asteroid 433 Eros". In: *Nature* 413.6854, pp. 390–393.
- Yano, H et al. (2004). "Sampling Strategy and Curation Plan of 'Hayabusa' Asteroid Sample Return Mission". In: *Lunar and Planetary Science Conference*. Vol. 35.
- Yano, Hajime et al. (2006). "Touchdown of the Hayabusa spacecraft at the Muses Sea on Itokawa". In: *Science* 312.5778, pp. 1350–1353.
- Yáñez, D García, Cuartielles, JP Sánchez, and McInnes, Colin R (2014). "Passive sorting of asteroid material using solar radiation pressure". In: *Journal of Guidance, Control, and Dynamics*.

Appendices

A

EXTRA FIGURES

This appendix contains figures which are used to support the explanation of certain results, arguments and conclusions in the main part of the Thesis report.

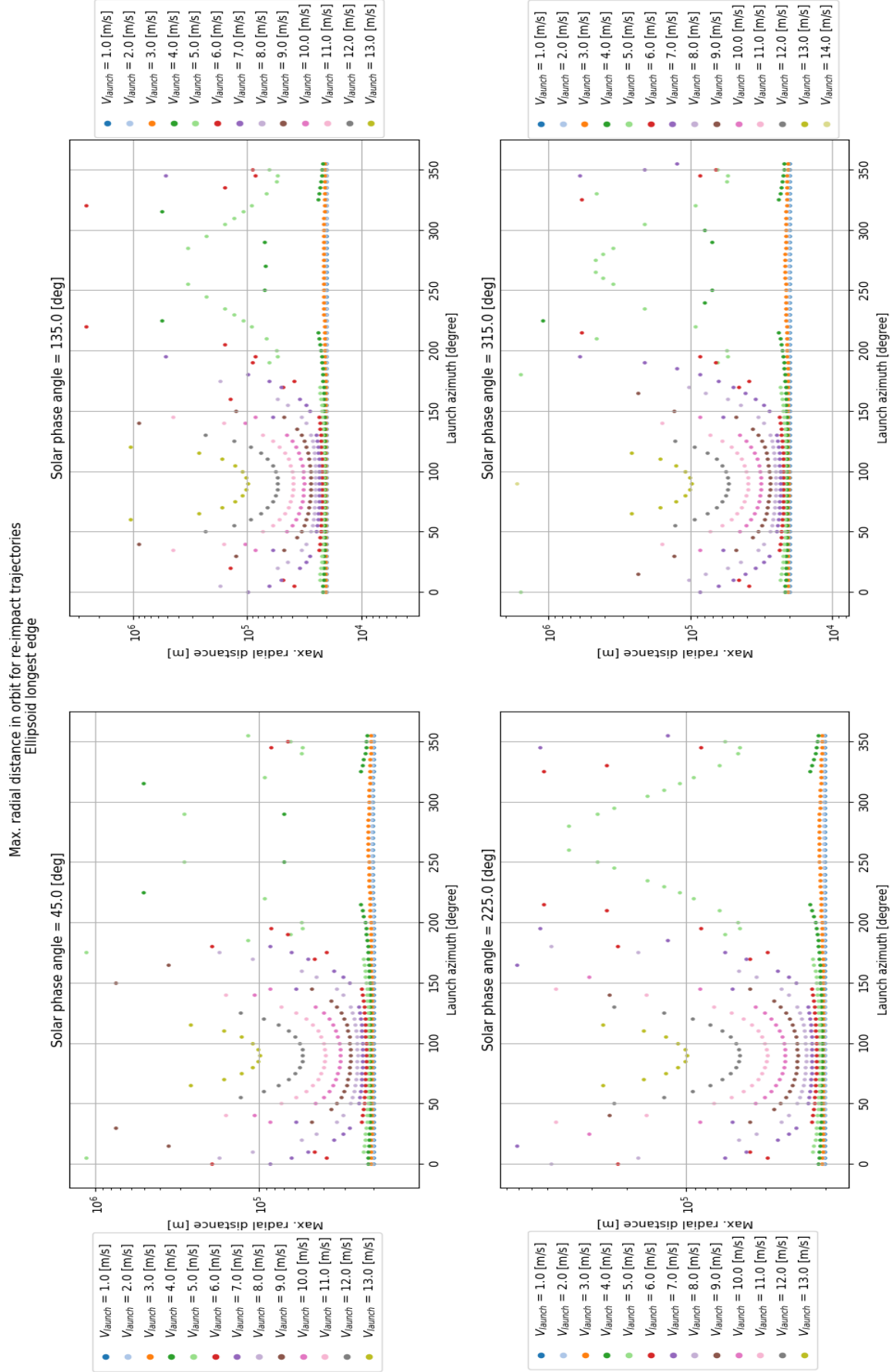
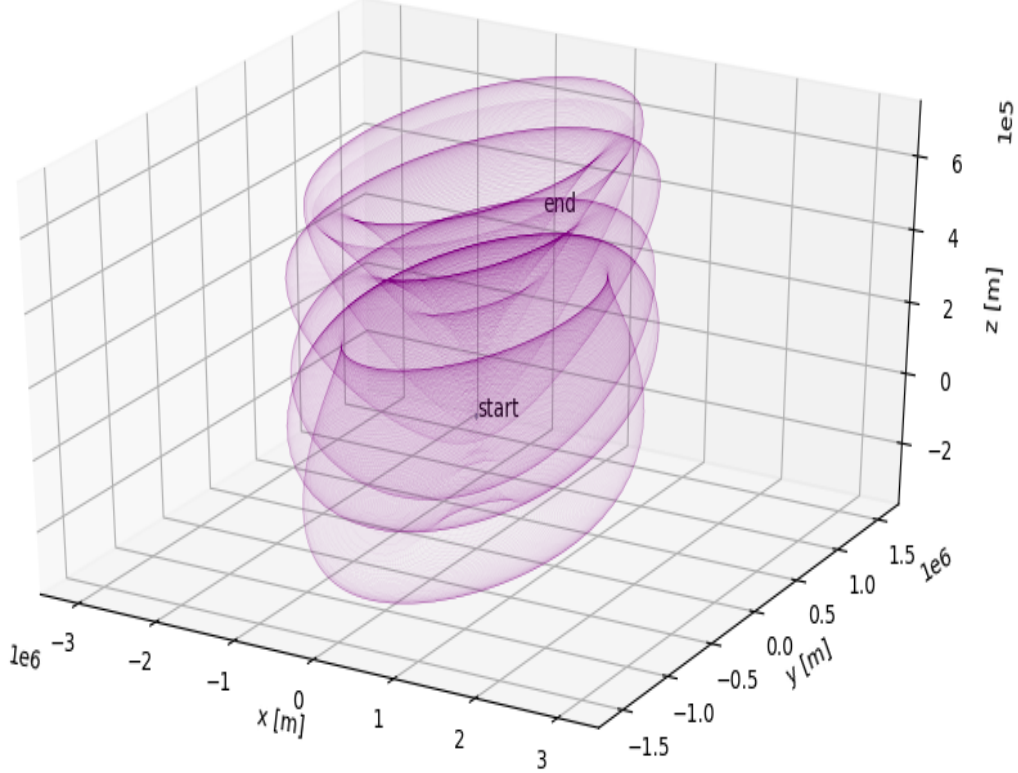


Figure A.1: Maximum radial distance (from the centre of the asteroid) attained by the regolith in orbit for different launch velocities and launch azimuths. The particles were launched from the longest edge of the ellipsoid (asteroid). Plots are for particle code LoGSP-1 and only for the re-impact scenario.

Particle trajectory around asteroid Eros (Body frame)
 $V_{initial}=10.0[\text{m/s}]$, Launch azimuth=45.0[deg], time=269.996608796[day(s)]



Particle trajectory around asteroid Eros (Inertial frame)
 $V_{initial}=10.0[\text{m/s}]$, Launch azimuth=45.0[deg], time=269.996608796[day(s)]

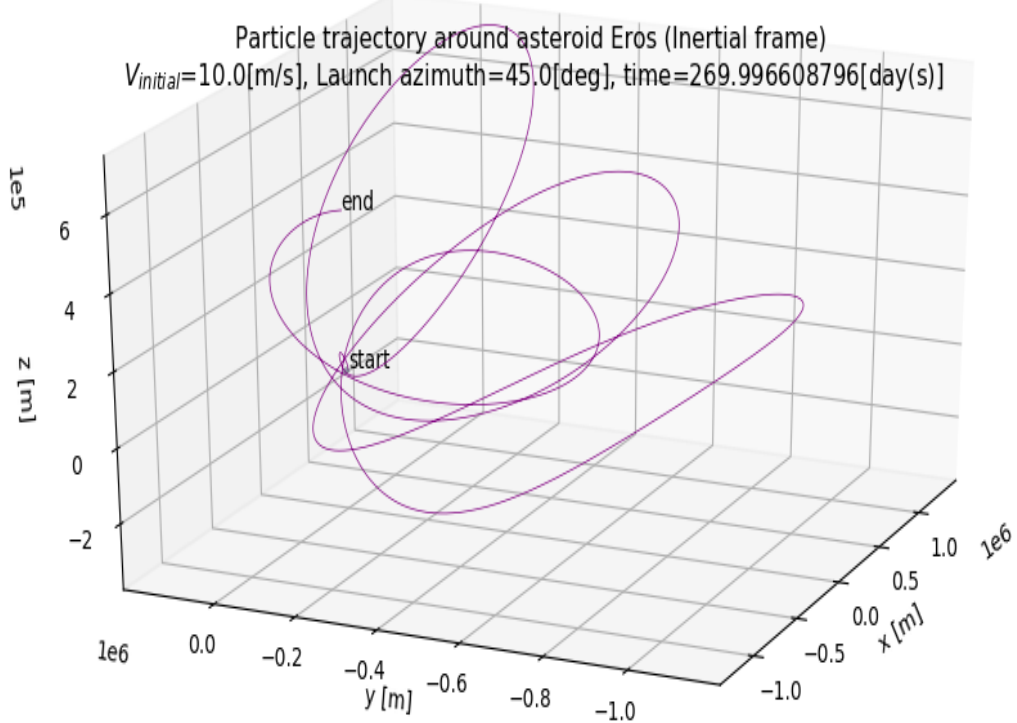


Figure A.2: 3D trajectory of capture regolith for case number 5 in Table 4.2. Particle code LoGSP-1.

Particle trajectory projection around asteroid Eros (Body fixed frame)
 $V_{initial}=10.0[\text{m/s}]$, Launch azimuth=45.0[deg], time=6479.91861111[hrs]

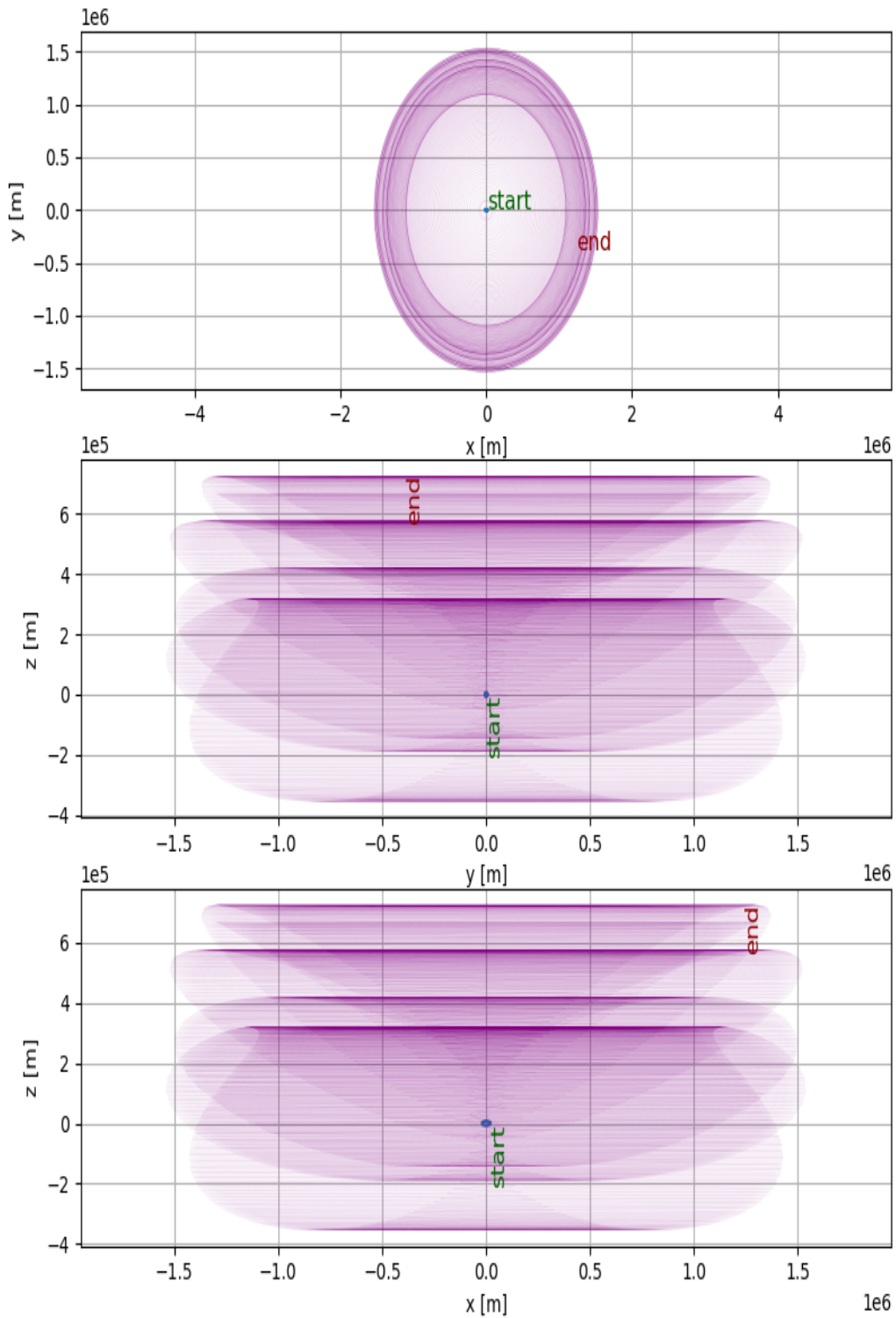


Figure A.3: 2D rotating frame trajectory of capture regolith for case number 5 in Table 4.2. Particle code LoGSP-1.

Particle trajectory around asteroid Eros (Body frame)
 $V_{initial}=8.0[\text{m/s}]$, Launch azimuth=165.0[deg], time=269.998056713[day(s)]

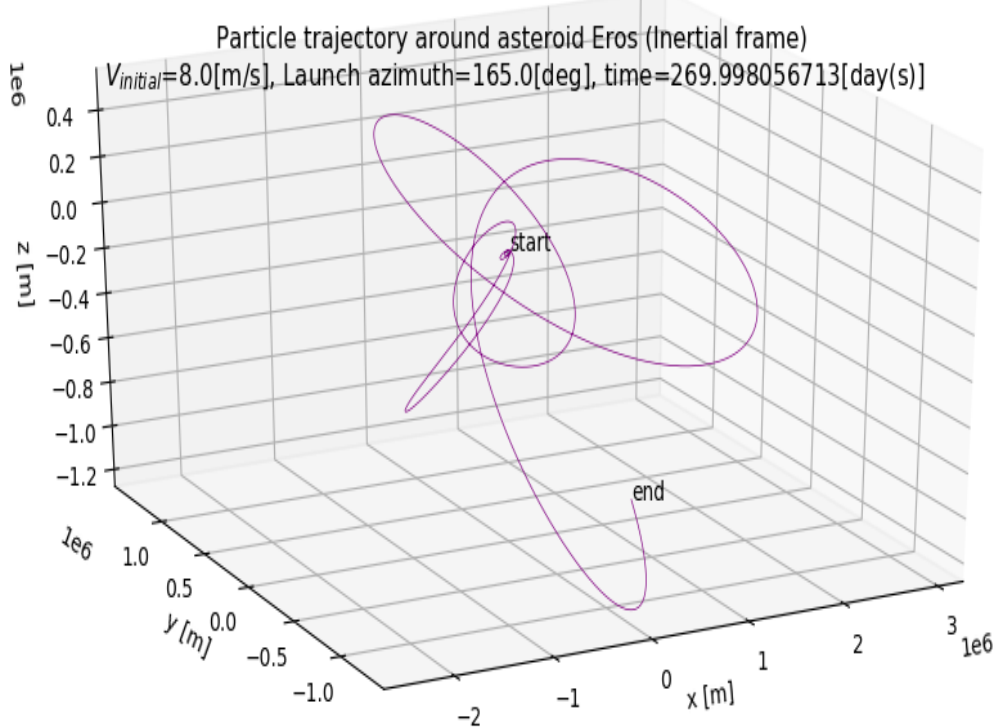
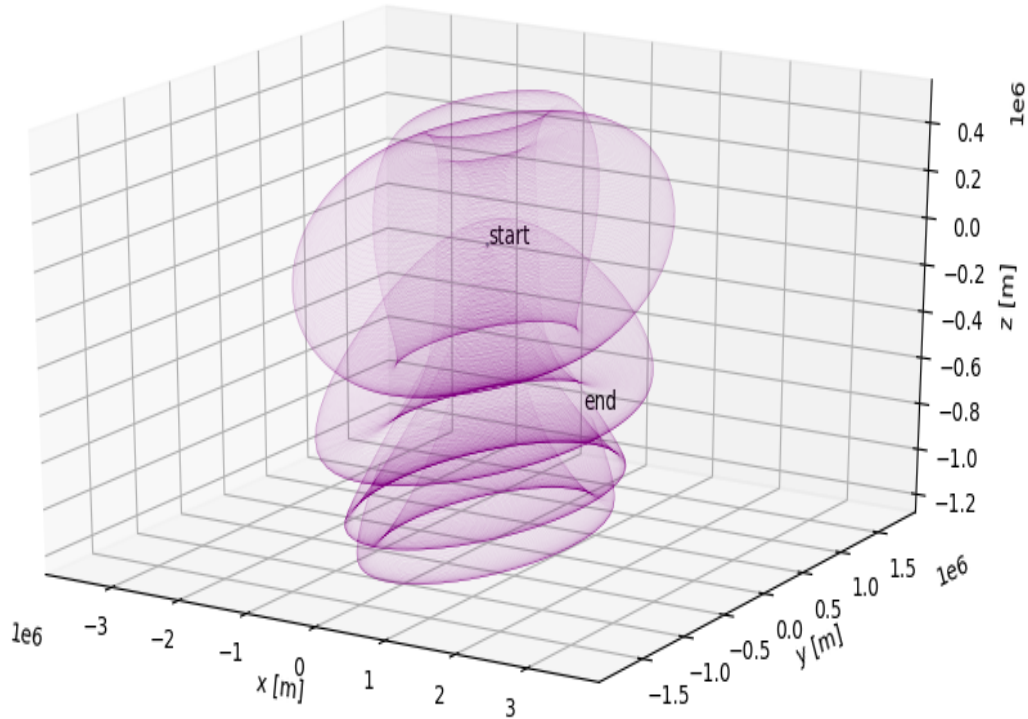


Figure A.4: 3D trajectory of capture regolith for case number 5 in Table 4.2. Particle code LoGSP-1.

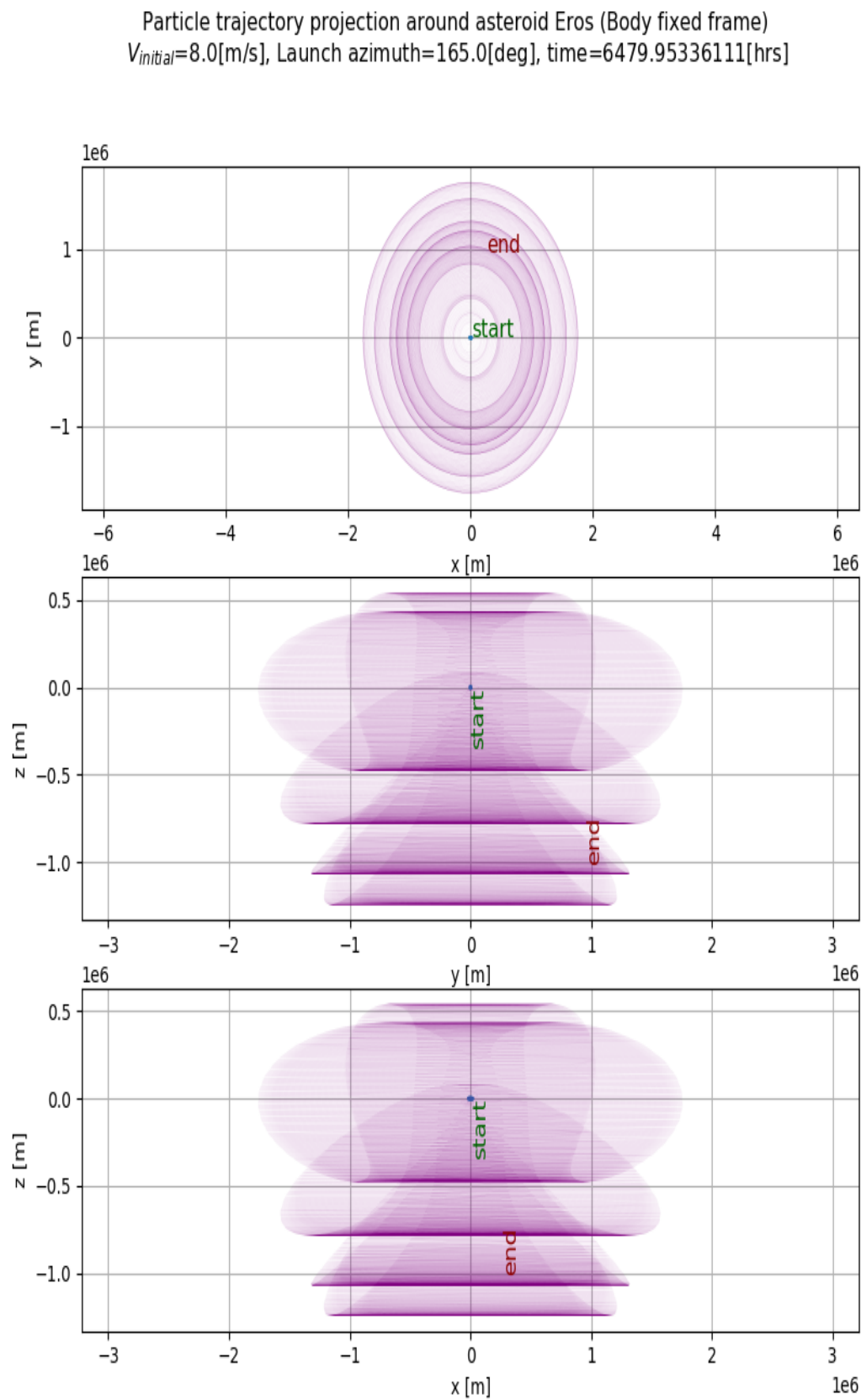


Figure A.5: 2D rotating frame trajectory of capture regolith for case number 8 in Table 4.2. Particle code LoGSP-1.